AD-A258 641

AEROSPACE REPORT NO.
ATR-91(7186)-2

Formation of Auroral Arcs via Magnetosphere-Ionosphere Coupling

Prepared by

L. R. LYONS
Space and Environment Technology Center
Technology Operations

DTIC
ELECTE
DEC 1 4 1992
S C D

15 September 1992

Prepared for

NATIONAL SCIENCE FOUNDATION
Washington, DC 20550

Grant No. ATM88-00602

Engineering and Technology Group

THE AEROSPACE CORPORATION
El Segundo, California

92-31326

PUBLIC RELEASE IS AUTHORIZED

92 12 14 006

TECHNOLOGY OPERATIONS

The Aerospace Corporation functions as an "architect-engineer" for national security programs, specializing in advanced military space systems. The Corporation's Technology Operations supports the effective and timely development and operation of national security systems through scientific research and the application of advanced technology. Vital to the success of the Corporation is the technical staff's wide-ranging expertise and its ability to stay abreast of new technological developments and program support issues associated with rapidly evolving space systems. Contributing capabilities are provided by these individual Technology Centers:

Electronics Technology Center: Microelectronics, solid-state device physics, VLSI reliability, compound semiconductors, radiation hardening, data storage technologies, infrared detector devices and testing; electro-optics, quantum electronics, solid-state lasers, optical propagation and communications; cw and pulsed chemical laser development, optical resonators, beam control, atmospheric propagation, and laser effects and countermeasures; atomic frequency standards, applied laser spectroscopy, laser chemistry, laser optoelectronics, phase conjugation and coherent imaging, solar cell physics, battery electrochemistry, battery testing and evaluation.

Mechanics and Materials Technology Center: Evaluation and characterization of new materials: metals, alloys, ceramics, polymers and their composites, and new forms of carbon; development and analysis of thin films and deposition techniques; nondestructive evaluation, component failure analysis and reliability; fracture mechanics and stress corrosion; development and evaluation of hardened components; analysis and evaluation of materials at cryogenic and elevated temperatures; launch vehicle and reentry fluid mechanics, heat transfer and flight dynamics; chemical and electric propulsion; spacecraft structural mechanics, spacecraft survivability and vulnerability assessment; contamination, thermal and structural control; high temperature thermomechanics, gas kinetics and radiation; lubrication and surface phenomena.

Space and Environment Technology Center: Magnetospheric, auroral and cosmic ray physics, wave-particle interactions, magnetospheric plasma waves; atmospheric and ionospheric physics, density and composition of the upper atmosphere, remote sensing using atmospheric radiation; solar physics, infrared astronomy, infrared signature analysis; effects of solar activity, magnetic storms and nuclear explosions on the earth's atmosphere, ionosphere and magnetosphere; effects of electromagnetic and particulate radiations on space systems; space instrumentation; propellant chemistry, chemical dynamics, environmental chemistry, trace detection; atmospheric chemical reactions, atmospheric optics, light scattering, state-specific chemical reactions and radiative signatures of missile plumes, and sensor out-of-field-of-view rejection.

Aerospace Report No.
ATR-91(7186)-2

FORMATION OF AURORAL ARCS VIA MAGNETOSPHERE-IONOSPHERE COUPLING

Prepared by

L. R. Lyons
Space and Environment Technology Center
Technology Operations

15 September 1992

Engineering and Technology Group
THE AEROSPACE CORPORATION
El Segundo, CA 90245-4691

Prepared for

NATIONAL SCIENCE FOUNDATION
Washington, DC 20550

Grant No. ATM88-00602

PUBLIC RELEASE IS AUTHORIZED

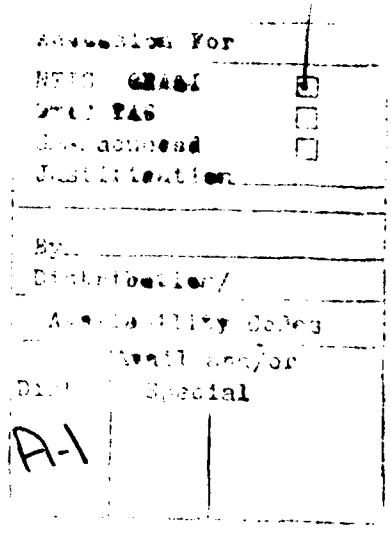

FORMATION OF AURORAL ARCS VIA
MAGNETOSPHERE-IONOSPHERE COUPLING

Prepared

L. R. Lyons

Approved

J. B. Blake, Director
Space Particles and Fields Department

A. B. Christensen, Principal Director
Space and Environment Technology Center

NOTE

The material reproduced in this report originally appeared in *Reviews of Geophysics*. The ATR is published to document the work for the corporate record.

FORMATION OF AURORAL ARCS VIA MAGNETOSPHERE-IONOSPHERE COUPLING

L. R. Lyons
Space and Environment Technology Center
The Aerospace Corporation
Los Angeles, California

Abstract. Brilliant displays of light are visible within a polar band of latitudes that surround each of the Earth's geomagnetic poles. These emissions are known as the aurora, and they are a dramatic consequence of the electromagnetic interaction between the Sun and the Earth. Energy is carried from the Sun by the plasma of the solar wind. This plasma impinges upon the magnetic field of the Earth and powers a wide range of electrodynamical phenomena that include the aurora. The aurora itself results from electrons that first are energized at very high altitudes by the solar wind-Earth interactions and then travel down magnetic field lines until they hit the atmosphere. In this tutorial I discuss the basic physical processes that lead to the energization of these electrons and thus to the aurora.

1. INTRODUCTION

A region of visible aurora generally encircles each of the Earth's polar caps [*Feldstein*, 1963; *Akasofu*, 1977]. These regions occur within the auroral zones, and they are typically a few degrees in latitude wide and lie between about 65° and 75° geomagnetic latitude. (Coordinates based on the geomagnetic field, rather than geographic coordinates, are generally used in magnetospheric and ionospheric physics.) While the auroral zones were initially identified from ground observations, aurora encircling the Earth within the auroral zones have now been dramatically seen in images from space. (See, for example, *Anger et al.* [1987] and subsequent papers in the same issue of *Geophysical Research Letters*, as well as *Frank and Craven* [1988].) The visible light of the aurora is emitted from altitudes between about 100 and 200 km and is a result of energetic particles impinging on the atmosphere from above. (Optical emissions from auroras are reviewed by *Vallance Jones* [1974].) In this tutorial I describe the basic physical processes that lead to the formation of auroral arcs, which are the most dramatic features of the auroral zones.

The Earth and its magnetic field are immersed in a plasma consisting of ions and electrons that flows outward from the Sun. This flowing plasma, called the solar wind, reaches the orbit of the Earth with a velocity V_{SW} that is typically 300–500 km/s and a density that is typically $5–10 \times 10^6$ m^{-3}. The magnetic field of the Sun is imbedded within the solar wind, and it extends throughout the interplanetary medium. At the orbit of the Earth the strength of this interplanetary field is about 5–10 nT. An electric field E is also associated with the solar wind and is given by $\mathbf{E} = -\mathbf{V}_{SW} \times \mathbf{B}$ in the frame of reference of the Earth, where B is the magnetic field. (See *Holzer* [1979] for a review of the physics of the solar wind.)

Solar energy and plasma are transferred to the Earth's environment by interactions of the solar wind with the geomagnetic field. These interactions occur kinetically via the energy of the solar wind particles and electrodynamically via the interplanetary magnetic and electric fields. Electrodynamic interactions cause the interplanetary electric field to extend onto the geomagnetic field. This electric field is transmitted along geomagnetic field lines to the ionosphere, which is highly conducting at altitudes between ~120 and 150 km. The combination of electric field and high-conductivity causes significant currents to flow in the ionosphere. Because the conductivity is governed by collisions between charged ionospheric particles and neutral atmospheric particles, the ionospheric currents are affected by properties and motion of the neutral atmosphere.

These ionospheric currents are most intense in the auroral zones, and they lead to the formation of auroral arcs. Here I first describe the geomagnetic interactions with the solar wind that lead to the large-scale electric field that maps along geomagnetic field lines to the ionosphere. I then discuss the ionospheric currents driven by this electric field, the formation of auroral arcs in association with these currents, and the effects of neutral winds on auroral electrodynamics.

Copyright 1992 by the American Geophysical Union.

8755-1209/92/92RG-00002 $15.00

Reviews of Geophysics, 30, 2 / May 1992
pages 93–112
Paper number 92RG00002

GLOSSARY

Anomalous resistivity: Resistivity caused by charged particle interactions with plasma waves.

Auroral arc: See discrete auroral arc.

Auroral zones: Approximately circular regions a few degrees wide that surround the geomagnetic poles near 70° geomagnetic latitude where observable auroras are most common.

Convection: Flow of plasma throughout the magnetosphere that is driven by the solar wind.

Diffuse aurora: Aurora formed by the precipitation into the atmosphere of geomagnetically trapped particles that are not accelerated by field-aligned electric fields. Diffuse auroras tend to be broader in latitudinal extend and less spatially structured than discrete auroral arcs.

Discrete auroral arc: Aurora formed by the precipitation into the atmosphere of electrons that have been accelerated by field-aligned electric fields. Such auroras tend to be narrow in latitudinal extend (approximately one to tens of kilometers), but they can extend large distances in longitude around the Earth.

Field aligned: Aligned along magnetic field lines.

Geomagnetic latitude: Latitude based on the Earth's magnetic axis rather than its geographic axis.

Gyroradius: Radius of the circular motion of charged particles about a magnetic field.

Gyroviscosity: A momentum transfer in a collisionless plasma that acts like viscosity. It depends upon changes in the magnitude of a particle gyroradius over the spatial scale of the gyroradius and can be expressed in terms of spatial derivatives of the off-diagonal elements of the pressure tensor.

Hall current: Component of the ionospheric current in the direction of $\mathbf{B} \times \mathbf{E}$.

Harang discontinuity: A reversal in magnetospheric plasma flow that has the same sense as the duskside convection reversal. In the ionosphere it lies near midnight and equatorward of the dawnside convection reversal.

Height-integrated current (conductivity): Current (conductivity) integrated over the height of the ionosphere.

Ionosphere: Region of enhanced ionization that surrounds the Earth at altitudes between ~75 and 1000 km altitude.

Magnetopause: Current layer that to a large extent separates the interplanetary magnetic field from the geomagnetic field.

Magnetosphere: Region of space within the magnetopause that is dominated by the geomagnetic field.

Neutral line: Magnetic x line along which $\mathbf{B} = 0$.

Pedersen current: Component of the ionospheric current in the direction of E.

Pitch angle: Angle between a particle's velocity and the magnetic field.

Precipitation: Loss of magnetospheric particles to the atmosphere by collisions at the low-altitude ends of magnetic field lines.

Reconnection electric field: Electric field along the boundary between open and closed geomagnetic field lines.

Solar wind: Plasma that flows outward from the Sun.

2. FORMATION OF THE MAGNETOSPHERIC ELECTRIC FIELD

The kinetic interaction between the solar wind and the geomagnetic field leads to the formation of a current layer that is referred to as the magnetopause. This current shields a large portion of the interplanetary magnetic field from the region interior to the magnetopause. As a result, the magnetopause is a sharp boundary that separates the interplanetary medium from a region of space that is dominated by the geomagnetic field and is referred to as the magnetosphere. The solar wind flow compresses the magnetosphere on the dayside and forms a long magnetospheric tail on the nightside. An illustration of the magnetopause and of magnetic field lines within, and in the vicinity of, the magnetosphere is shown in Figure 1.

Shielding of the interplanetary magnetic field by the magnetopause current is not complete, and a portion of the interplanetary field crosses the magnetopause and connects with the geomagnetic field. This connection between magnetic fields is illustrated in Figure 1 for the case when the interplanetary field is directed southward. (The case of a southward directed interplanetary field is simplest to illustrate; however, similar connection between the fields occurs for other orientations as discussed later.) Note that the region of connected field maps to the Earth as approximately circular regions over each polar cap. Such field lines are referred to as open. Magnetic field lines emanating from the Earth at lower latitudes are closed. They cross the equatorial plane and return to the Earth without connecting with the interplanetary field. The auroral zones lie in the vicinity of the boundary between open and closed magnetic field lines.

Electric Field Distribution

As illustrated in Figure 1, the solar wind flows across the interplanetary portion of the open polar cap magnetic field lines, and the interplanetary electric field is directed normal to these field lines and to the solar wind. The electric conductivity is high along geomagnetic field lines, so that to a very good approximation they can be approximated as equipotentials. Thus the interplanetary electric field maps along field lines to the polar caps, where it is directed in the dawn-to-dusk direction. While there are important exceptions to the equipotential assumption, as will be discussed later in connection with the formation of auroral arcs, the assumption is very good for large-scale electric field mappings such as we are considering here.

The interplanetary electric field has a value of about 3 mV/m, based on $V_{SW} = 400$ km/s and $B = 8$ nT. Also, it is

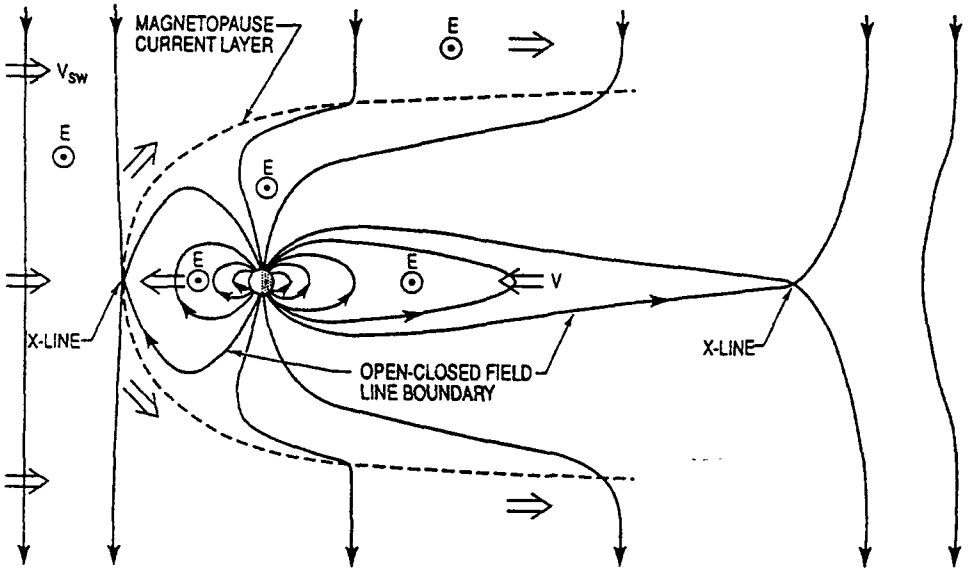

Figure 1. Illustration of magnetic and electric fields within, and in the vicinity of, the magnetosphere. Plasma flows outside (V_{SW}) and within (V) the magnetosphere are indicated.

known from satellite observations that the geomagnetic tail has a roughly circular cross section of diameter ~40 Earth radii (R_e). Thus if the entire interplanetary magnetic field were to penetrate the magnetopause, there would be a potential difference $\Delta\phi$ across the geomagnetic tail of about 800 kV. This potential difference would map along magnetic field lines to the polar cap ionosphere. The connection of interplanetary magnetic field lines with polar cap geomagnetic field lines for this condition is illustrated by the dashed lines in Figure 2. In the figure, field lines emanating from the Earth along the dawn-dusk meridian are projected onto the dawn-dusk meridian plane, and the mapping of the interplanetary electric field to the polar caps is shown by arrows in the dawn-to-dusk direction.

Electric field observations from satellites that cross the polar cap at ionospheric altitudes show that a dawn-to-dusk electric field often exists across the polar cap as expected from the mapping discussed above. Two examples of such observations are shown in Figure 3 [from *Heppner*, 1972]. However, the potential difference across the polar caps (the region where E_x is negative in Figure 3) is about 10 times less than the 800 kV that would result from a penetration of the entire interplanetary magnetic field across the magnetopause. This implies that only about 10% of the interplanetary field crosses the magnetopause [*Stern*, 1973]. The projection of polar cap field lines for this more realistic situation is shown by the solid lines in Figure 2. As is illustrated, most of the interplanetary magnetic field is diverted around the magnetosphere by the magnetopause currents.

Understanding why the fraction of the interplanetary field that penetrates is about 10% is a problem that has yet to be adequately solved. However, it is not surprising that the fraction is small, since the energy density of the solar flow is about 30 times greater than the energy density of the interplanetary magnetic field (based on protons flowing at 400 km/s, a density of 8×10^6 m^{-3}, and $B = 8 \times 10^{-9}$ T). It is also not surprising that some of the interplanetary field does penetrate, since otherwise the magnetopause currents would need to have the precise distribution required to shield all of the time-variable interplanetary field from the magnetosphere.

Under the assumption that the solar wind flow does not penetrate onto closed magnetic field lines the interplanetary electric field directly maps only to the region of open polar cap magnetic field. The boundary between open and closed field lines thus becomes charged, the charge being negative along the duskside of the boundary and positive on the dawnside as indicated in Figure 2. This charge separation gives rise to an electric field throughout the closed field line portion of the magnetosphere having a direction that is also indicated in Figure 2. The electric field on closed field lines near the equatorial plane is in the same direction as it is on open field lines over the poles; however, the relation $\mathbf{E} = -\mathbf{V} \times \mathbf{B}$ shows that the plasma flow is sunward near the equator, where B is northward, and antisunward over the poles.

The electric field and plasma flow in the equatorial plane is illustrated in Figure 4. Note that the charging of the dawnside and duskside of the open-closed field line boundary requires that there be an electric field along the boundary. This electric field is referred to as the reconnection electric field. Such an electric field is a consequence

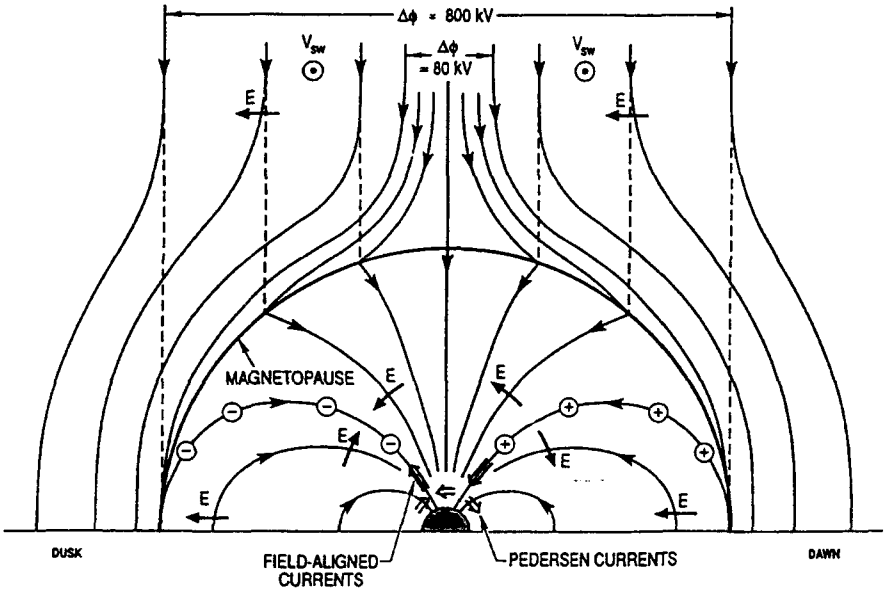

Figure 2. Mapping of magnetic field lines emanating from the dawn-dusk meridian of the polar caps to the interplanetary medium as projected onto the dawn-dusk meridian plane. Dashed lines illustrate the mapping under the assumption that the entire interplanetary magnetic field penetrates the magnetopause. Solid lines illustrate the mapping under the more realistic assumption that only about 10% of the interplanetary field penetrates the magnetopause and that the majority of the interplanetary field is diverted around the magnetosphere. The magnetospheric electric field and charges along the boundary between open and closed magnetic field lines are also shown. Ionospheric Pedersen currents and the field-aligned currents driven by the magnetospheric electric field are indicated by open arrows.

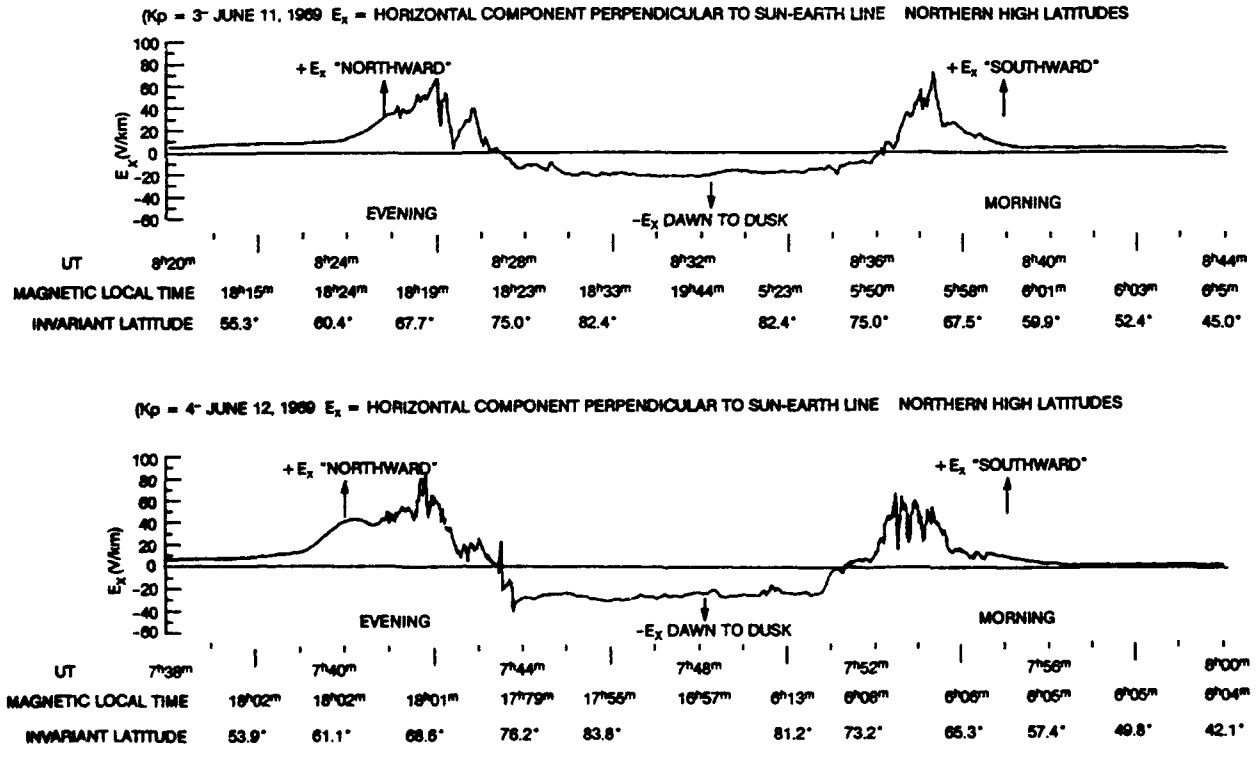

Figure 3. Two typical examples of the electric field observed approximately along the dusk-dawn meridian from low-altitude passes of a satellite over the polar caps [from *Heppner*, 1972].

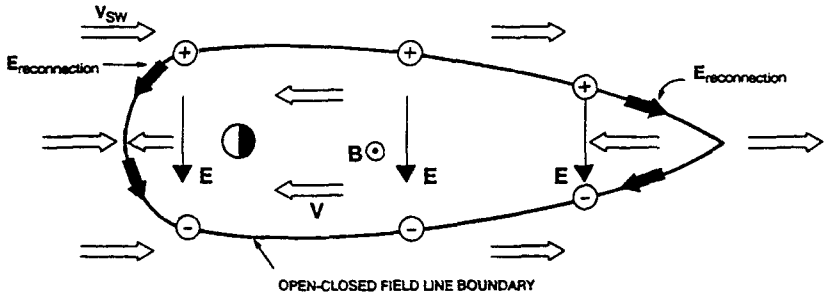

Figure 4. Illustration of electric field and plasma flow in the equatorial plane. Charging of the boundary between open and closed magnetic field lines requires that there be an electric field, referred as the reconnection electric field, along that boundary.

of the connection between the interplanetary and geomagnetic fields, and it is associated with the extension of the interplanetary electric field into the closed magnetic field portion of the magnetosphere. The reconnection electric field maps along the open-closed field line boundary from the equatorial plane to the ionosphere and is directed so as to transfer plasma across the boundary from closed to open field lines on the dayside and from open to closed field lines on the nightside. This result can be seen in Figure 1 by mapping the dawn-to-dusk electric field along the open-closed field line boundary to near the Earth's surface and applying the relation $\mathbf{E} = -\mathbf{V} \times \mathbf{B}$.

The electric potentials and plasma flows map to the ionosphere as illustrated in Figure 5. This figure shows electric equipotentials as seen looking down over the northern polar cap. Plasma flow follows the equipotential contours in the direction given by $\mathbf{E} = -\mathbf{V} \times \mathbf{B}$, being antisunward over the polar caps and returning toward the dayside at lower latitudes. The flow crosses the open-closed field line boundary with a velocity determined by the reconnection electric field. The charges on the boundary extend to the ionosphere, keeping the boundary field lines as equipotentials, and are indicated in Figure 5. These charges are critical to the formation of auroral arcs.

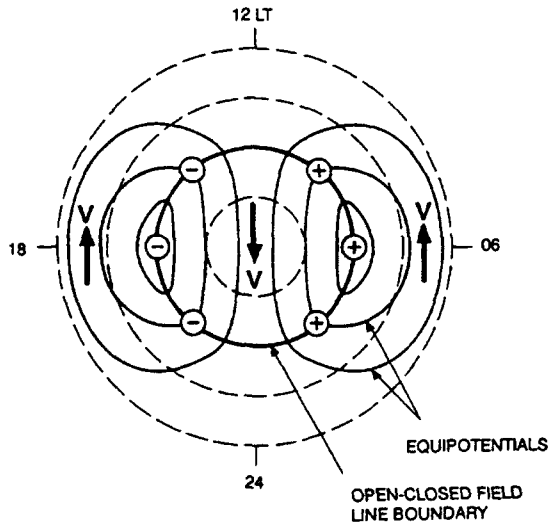

Figure 5. Mapping of magnetospheric electric potentials and plasma flows to the ionosphere as seen looking down over the northern polar cap.

The overall flow pattern is referred to as magnetospheric convection, and the qualitative pattern shown in Figure 5 is the most common pattern observed within the ionosphere. Measurements of the instantaneous electric field distribution over an entire polar cap are not obtainable with presently available instrumentation; however, the distribution has been inferred from observations in a number of ways. The observations that have been used include the alignment of auroral forms and the motion of visual irregularities along the forms [*Davis*, 1960, 1962], the magnetic effects of the ionospheric currents known as S_q^p (q for quiet, p for polar) [*Nagata and Kokubun*, 1962; *Nishida et al.*, 1966], direct satellite measurements of electric fields [*Cauffman and Gurnett*, 1971; *Heppner*, 1972; *Heppner and Maynard*, 1987; *Marklund et al.*, 1987; *Heelis*, 1988], and ground-based radar observations of ionospheric plasma flows [*Foster*, 1983; *de la Beaujardiere et al.*, 1985; *Foster et al.*, 1986].

The instantaneous potential distribution over an entire polar cap has been estimated by *Richmond et al.* [1988] using ground-based measurements of ionospheric plasma flows and currents that cover as much of the polar cap as possible. An example of their distributions is shown in Figure 6, which can be seen to be qualitatively similar to that in Figure 5. An electric field reversal extends essentially around the entire polar cap, with $\nabla \cdot \mathbf{E} < 0$ on the duskside and $\nabla \cdot \mathbf{E} > 0$ on the dawnside. The duskside reversal extends equatorward of the dawnside reversal near midnight. This equatorward extension of the $\nabla \cdot \mathbf{E} < 0$ reversal is referred to as the Harang discontinuity. Bright auroral arcs are commonly observed in the vicinity of the duskside reversal and the Harang discontinuity.

Convection over the polar caps does vary from nearly antisunward flow in response to changes in the interplanetary magnetic field direction. Flow patterns are observed to become curved when the y component of the interplanetary field becomes significant (y lies in the ecliptic plane and is directed normal to the Earth-Sun line), with the sense of the curvature dependent on the sign of B_y [*Svalgaard*, 1968, 1973; *Mansurov*, 1969; *Heppner*, 1972; *Heelis et al.*, 1983; *Heelis*, 1984]. When the interplanetary field becomes strongly northward ($B_z > 0$), the flow

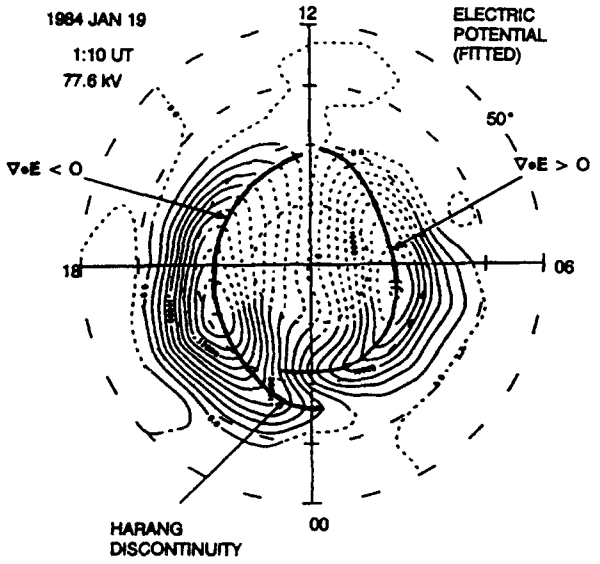

Figure 6. Estimated electric potential pattern over an entire polar cap obtained by *Richmond et al.* [1988] from ground-based measurements of ionospheric electric fields and currents that cover as much of the polar cap as possible. Equipotential contours are dashed where estimated electric field uncertainties exceed 50%.

becomes sunward across the center of the polar cap but remains antisunward along the dawn and dusk portion of the polar cap [*Maezawa*, 1976; *Burke et al.*, 1979; *Zanetti et al.*, 1984].

These variations of the polar cap flow patterns can be explained by the connection of the interplanetary and geomagnetic fields in the manner described above for the case of a purely southward directed field [*Stern*, 1973; *Crooker*, 1979; *Longenecker and Roederer*, 1981; *Lyons*, 1985; *Toffeletto and Hill*, 1989]. As an illustration, we briefly consider the case where the interplanetary field has a strong northward component.

For simplicity we look at the addition of the Earth's field as represented by a dipole and an interplanetary field with $B_z = 10$ nT and $B_x = -10$ nT. Figure 7 shows field lines in the noon-midnight meridian plane, and Figure 8 shows field lines emanating from the Earth along the dawn-dusk meridian plane as mapped into that plane. The interplanetary electric field in this case is directed in the dusk-to-dawn direction, which is opposite to its direction for a southward interplanetary field. Along the noon-midnight meridian, the dusk-to-dawn electric field maps into the polar cap ionosphere and gives sunward convection (Figure 7). Toward dawn and dusk, on the other hand, the magnetic field mapping reverses the direction of the electric field resulting in antisunward convection (Figure 8). The convection pattern over the entire polar cap that is obtained from the superposition of a dipole field and an interplanetary field with $B_z > 0$ is shown in Figure 9 and is in qualitative agreement with observations. (The conver-

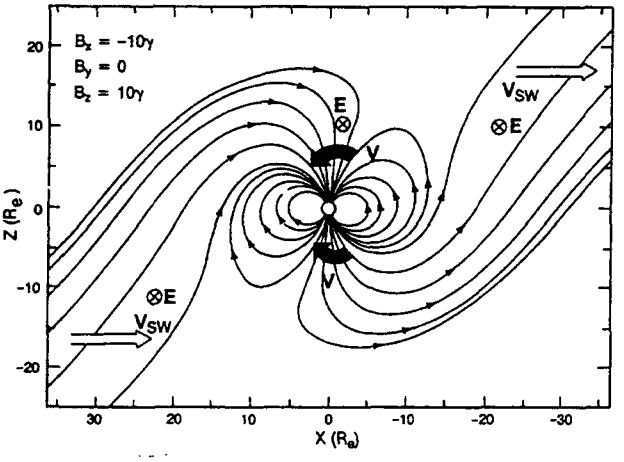

Figure 7. Magnetic field lines in the noon-midnight meridian plane as obtained from the addition of an interplanetary field with $B_x = -10$ nT, $B_y = 0$, and $B_z = 10$ nT and the Earth's field as represented by a dipole. Somewhat large magnitudes for B_x and B_z have been used in this figure and in Figure 8 in order to emphasize the geometry of the connection between the interplanetary and geomagnetic fields. The directions of the electric field E, the solar wind V_{SW}, and the polar cap plasma flow V are shown [from *Lyons*, 1985].

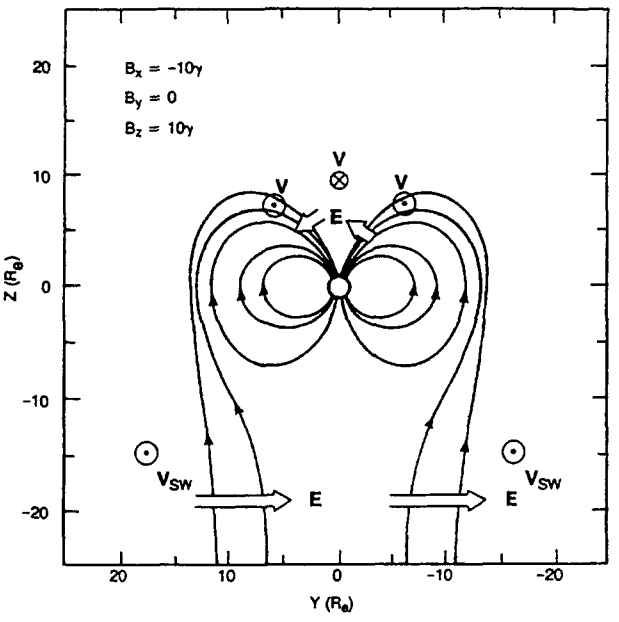

Figure 8. Magnetic field lines emanating from the Earth along the dawn-dusk meridian plane and mapped into that plane as obtained from the addition of an interplanetary field with $B_x = -10$ nT, $B_y = 0$, and $B_z = 10$ nT and the Earth's field as represented by a dipole. Only field lines near the northern hemisphere boundary between open and closed field lines are shown. The directions of the electric field E, the solar wind V_{SW}, and the polar cap plasma flow V are shown [from *Lyons*, 1985].

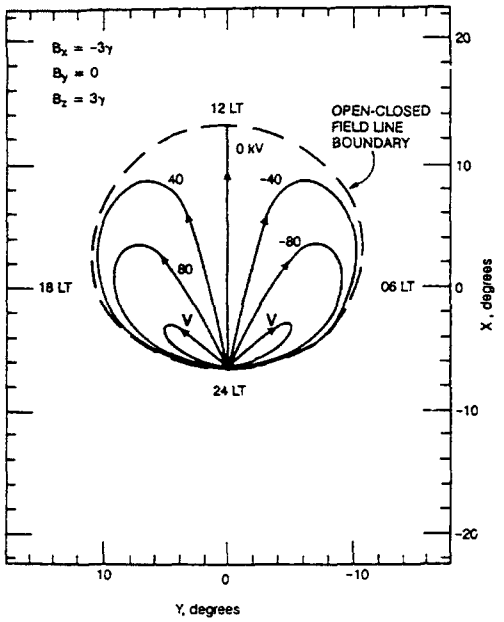

Figure 9. Equipotential contours across open, northern hemisphere, polar cap field lines as obtained from the addition of an interplanetary field with $B_x = -3$ nT, $B_y = 0$, and $B_z = 3$ nT and the Earth's field as represented by a dipole for a solar wind speed of 300 km/s. Arrows on the potential contours give the direction of plasma convection, and the dashed curve gives the boundary between open and closed magnetic field lines. Axes are labeled in degrees from the magnetic pole; actual distances are approximately 110 km per degree [from *Lyons*, 1985].

gence of the equipotential contours at a point along the open-closed field line boundary is an artifact of the magnetic field model and the assumption that all field lines are equipotentials, even where B is very weak. In reality, the potential contours will not converge to a point and will most likely cross the open-closed field line boundary.)

The interesting variation of the polar cap convective flow with the direction of the interplanetary field, which is readily explained by considering the connection between the geomagnetic and interplanetary fields, lends strong support to the contention that magnetospheric convection is driven primarily by solar wind flow across open polar cap field lines. For all orientations of the field this interaction leads to significant charges along the boundary between open and closed field lines, where $\nabla \cdot \mathbf{E} \neq 0$, as is shown in Figures 5 and 6. These charges are important for understanding magnetosphere-ionosphere interactions.

The foregoing discussion has been under the assumption that flowing solar wind plasma does not penetrate onto closed magnetic field lines. However, it has been proposed that such penetration of the solar wind occurs and can be sufficient to generate some of the antisunward flow over the polar caps [e. g., *Lemaire*, 1977; *Heikkila*, 1979; *Lundin*, 1987]. If this were the case, then part of the antisunward flow at the sides of the polar cap would be on closed magnetic field lines. This would move the reversal in the ionospheric flow direction, and the location of maximum charge density, to a position somewhat equatorward of the open-closed field line boundary. However, it would have little other direct effect on the phenomena discussed in this paper.

Force Balance Along Magnetic x Line

As shown in Figure 1, the boundary between open and closed magnetic field lines maps to a magnetic x line at the magnetopause. This x line extends around the entire magnetosphere. The reconnection electric field extends along the open-closed field line boundary so as to be directed along the x line. At any position along the x line, **B** must be either zero or directed along the x line. In either case it is clear that the relation $\mathbf{E} = -\mathbf{V} \times \mathbf{B}$, which is a basic assumption of ideal magnetohydrodynamics, cannot be valid anywhere along the x line where the reconnection electric field is nonzero. Since this electric field is critical to the transfer of mass and energy to the closed field line region of the magnetosphere, the physics of the region in the vicinity of an x line along which lies an electric field has become an important problem in magnetospheric physics.

In particular, the question of what forces balance the electric force along an x line is often considered. These forces can be evaluated using the generalized Ohm's law, which gives a relation between **E** and other quantities in a plasma. This equation, which is simply a combination of the electron and ion momentum equations, can be written [*Rossi and Olbert*, 1970]:

$$\mathbf{E} + \mathbf{V} \times \mathbf{B} = (m_e/e^2 n)[\partial \mathbf{J}/\partial t + \nabla \cdot (\mathbf{JV} - \mathbf{VJ}) + (\partial \mathbf{J}/\partial t)|_{coll}] + (1/en)[\mathbf{J} \times \mathbf{B} - \nabla \cdot \mathbf{P}_e] \quad (1)$$

Here e is the electronic charge, m_e is the electron mass, n is the electron density, **J** is the current density, $\mathbf{P}_e$ is the electron pressure tensor, and $(\partial \mathbf{J}/\partial t)|_{coll}$ represents the effects of particle collisions.

In many space physics applications the terms on the right-hand side of (1) are small compared to $\mathbf{V} \times \mathbf{B}$ and the approximation $\mathbf{E} + \mathbf{V} \times \mathbf{B} = 0$ can be applied [*Siscoe*, 1983]. However, this approximation precludes the existence of an electric field along a magnetic x line. In traditional reconnection theory the terms on the right-hand side of (1) are still neglected, but a term $\eta \mathbf{J}$ is included, so that

$$\mathbf{E} + \mathbf{V} \times \mathbf{B} = \eta \mathbf{J}$$

Here η represents a resistivity, and the problem becomes one of understanding the cause of the resistivity. For a collisionless plasma, η is referred to as anomalous resistivity, and it is often attributed to wave-particle interactions.

The term $\eta \mathbf{J}$ works quite well in collisional plasmas such as the ionosphere if η is replaced by a tensor.

However, it is very difficult to justify the use of such a term in a collisionless plasma. Recently, however, there has become increased interest in collisionless reconnection, where the $\eta\mathbf{J}$ term is not included and the condition $\mathbf{E} + \mathbf{V} \times \mathbf{B} = 0$ is violated as a result of the finite inertia of individual particles [e.g., *Speiser*, 1970; *Coroniti*, 1985; *Burkhart et al.*, 1990]. These inertial effects are included in the terms on the right-hand side of (1). Thus it is useful to look at the magnitude of these terms. We do this by first evaluating the magnitudes at the center of the magnetopause current layer. Then, for simplicity, we assume that the magnetic x line is a neutral line and examine the terms as $B \rightarrow 0$.

We take an electron thermal energy of 100 eV, so that $P_e = nkT_e \sim en(100\ \text{eV})$, a component of B normal to the current layer $B_n = 0.8 \times 10^{-9}$ T, and a density $n = 10^6$ m^{-3}. Letting there be a scale length $L = 2 \times 10^6$ m for changes along the direction normal to the current layer, and a change in the magnetic field across the current layer given by $\Delta B = 4 \times 10^{-8}$ T, we obtain $J = \Delta B/(\mu_0 L) = 1.6 \times 10^{-8}$ A/m^2. We also take $V = 3 \times 10^5$ m/s and a time scale for current changes of $\Delta t = 600$ s. To be significant, a term on the right-hand side of (1) needs to have a magnitude comparable to that of the electric field. As an estimate for E, we assume that a 60-kV potential difference is distributed along a magnetopause path length of 60 R_e. We assume uniformity along the direction of the current and that $\mathbf{E}$ is parallel to $\mathbf{J}$.

With the above parameters, we have

$$E \sim 1.6 \times 10^{-4}\ \text{V/m}$$

$$(m_e/e^2 n)[\partial J/\partial t] \sim (m_e/e^2 n)J/\Delta t = 9.7 \times 10^{-10} \ll E$$

$$(m_e/e^2 n)|\nabla \cdot \mathbf{JV}| \sim (m_e/e^2 n)|\nabla \cdot \mathbf{VJ}| \sim (m_e/e^2 n)VJ/L = 8.5 \times 10^{-8} \ll E$$

$$(1/en)|\mathbf{J} \times \mathbf{B}| \sim (1/en)JB_n = 8.0 \times 10^{-5} \sim E$$

$$(1/en)\,\nabla \cdot \mathbf{P}_e \sim (1/en)P_e/L = 5.0 \times 10^{-5} \sim E$$

Thus the $\partial\mathbf{J}/\partial t$, $\mathbf{JV}$, and $\mathbf{VJ}$ terms can be neglected in the generalized Ohm's law. However, the $\mathbf{J} \times \mathbf{B}$ and $\nabla \cdot \mathbf{P}_e$ terms are not negligible.

Taking $\mathbf{E}$ to be in the y direction, we have that the component of $\nabla \cdot \mathbf{P}_e$ in the direction of $\mathbf{E}$

$$(\nabla \cdot \mathbf{P}_e)_y = (\partial P_{xy}/\partial x) + (\partial P_{zy}/\partial z),$$

which depends on the changes in the magnitude of the electron gyroradius over the spatial scale of the gyroradius. Well away from a neutral line, these gradients are small. Using the definitions, $\mathbf{V} = (m_e\mathbf{V}_e + m_i\mathbf{V}_i)/(m_e + m_i)$, $\mathbf{J} = ne(\mathbf{V}_i - \mathbf{V}_e)$, and taking $m_e/m_i \ll 1$ (where subscript "i" refers to ions), we are left with

$$\mathbf{E} = -\mathbf{V} \times \mathbf{B} + (1/en)(\mathbf{J} \times \mathbf{B}) = -\mathbf{V}_e \times \mathbf{B}.$$

well away from a neutral line. Thus electrons move with the electric field drift velocity, but ions are free to move in the direction of $\mathbf{J}$. It is this ion motion that forms the magnetopause current layer.

The term $\mathbf{V}_e \times \mathbf{B} \rightarrow 0$ at a neutral line. However, the spatial variation of the electron gyroradius becomes significant as $B \rightarrow 0$ so that $(\nabla \cdot \mathbf{P}_e)_y$ becomes significant and

$$enE = = -(\partial P_{xy}/\partial x) - (\partial P_{zy}/\partial z), \qquad (2)$$

in the vicinity of a neutral line.

Equation (2) was derived by *Vasyliunas* [1975] and shows that the divergence of the electron pressure tensor must provide the force needed to balance the electric force along a neutral line in a collisionless plasma. In particular, it is the spatial variation of the off-diagonal elements of the pressure tensor that are critical for the force balance [*Vasyliunas*, 1975; *Sonnerup*, 1979]. The gradient of these off-diagonal elements represents a transfer of y momentum in the x and z directions that results from spatial gradients of the electron gyroradius. This momentum transfer has been referred to as gyroviscosity by *Sonnerup* [1988].

Dungey [1988] evaluated electron motion in the vicinity of a neutral line and proposed that the electron gyroviscosity could be sufficient to balance the electric force along a neutral line when magnetic field gradients are large. On the basis of this suggestion, *Lyons and Pridmore-Brown* [1990] evaluated the forces near a neutral line using a simplified model. Their results imply that gyroviscosity can in general balance the electric force at a neutral line in a collisionless plasma, independent of the plasma particle and field parameters. Thus only phenomena that are included in the collisionless generalized Ohm's law are required for there to be a finite reconnection electric field in a collisionless plasma. Additional processes, such as anomalous resistivity, are not necessary.

3. IONOSPHERIC CURRENTS AND THE FORMATION OF AURORAL ARCS

Ionospheric Current-Electric Field Relations

The magnetospheric convection electric field affects the motion of charged particles in the ionosphere. However, in the ionosphere the frequency of collisions between charged particles and neutrals becomes comparable to the charged particle gyrofrequency (the frequency of circular motion in the plane normal to the magnetic field). The collisions interrupt the particle drift in the direction normal to $\mathbf{E}$ and cause a differential motion between electrons and ions. As a result, currents flow in the ionosphere in the plane normal to $\mathbf{B}$. It is often convenient to divide this current into two components, the Pedersen current $J_p = \sigma_p E$ in the direction of $\mathbf{E}$ and the Hall current $J_H = \sigma_H E$ in the direction of $\mathbf{B} \times \mathbf{E}$. The constants σ_p and σ_H are known as the Pedersen and Hall conductivities, respectively. They depend on the ionospheric collision frequencies as discussed by *Rishbeth and Garriott* [1969].

It is convenient to treat the ionosphere as a conducting shell and to thus integrate the ionospheric currents and conductivities over the height z of the ionosphere. Doing this allows us to define height-integrated quantities $\mathbf{I} = \int \mathbf{J}\, dz$ and $\Sigma = \int \sigma\, dz$ such that

$$\mathbf{I}_P = \Sigma_P \mathbf{E}$$

$$\mathbf{I}_H = -\Sigma_H \mathbf{E} \times \mathbf{B}/B$$

Field-aligned currents (currents in the direction of the magnetic field) $J_\parallel$ flow from the ionosphere to the magnetosphere and are critical to the formation of auroral arcs. Current continuity in the ionosphere requires that $\nabla \cdot \mathbf{J} = 0$, which allows us to relate $J_\parallel$ to the divergence of the height-integrated ionospheric current. Assuming the geomagnetic field is vertical in the ionosphere (which is a good approximation in polar regions), we can relate $J_\parallel$ to the horizontal divergence ($\nabla_\perp$) of the height-integrated ionospheric currents:

$$J_\parallel = -\nabla_\perp \cdot \mathbf{I} = -\nabla_\perp \cdot \mathbf{I}_P - \nabla_\perp \cdot \mathbf{I}_H \qquad (3)$$

Using parameters typical of the auroral ionosphere ($\mathbf{E}_\perp \sim 10$ mV/m, $\nabla_\perp \cdot \mathbf{E}_\perp \sim \mathbf{E}_\perp/10$ km $= 10^{-6}$ V/m^2, $\Sigma_P \sim \Sigma_H \sim 10$ mhos, $J \sim \Sigma_P \mathbf{E}_\perp/30$ km $= 3 \times 10^{-7}$ A/m^2, $B = 5 \times 10^{-5}$ T, $\partial \mathbf{B}/\partial t \sim 500$ nT/250 s $= 2 \times 10^{-9}$ T/s) and neglecting spatial variations of the conductivities, we have

$$\nabla_\perp \cdot \mathbf{I}_P = \Sigma_P \nabla_\perp \cdot \mathbf{E}_\perp \sim 10^{-5}\ \text{A/m}^2$$

$$\nabla_\perp \cdot \mathbf{I}_H = -\Sigma_H [\mathbf{B} \cdot \nabla \times \mathbf{E}_\perp - \mathbf{E}_\perp \cdot \nabla \times \mathbf{B}]/B$$

$$= \Sigma_H [\mathbf{B} \cdot (\partial \mathbf{B}/\partial t) + \mu_0 \mathbf{E}_\perp \cdot \mathbf{J}]/B$$

$$\sim [2 \times 10^{-8} + 8 \times 10^{-10}]\ \text{A/m}^2 \ll \nabla_\perp \cdot \mathbf{I}_P$$

This shows that $\nabla_\perp \cdot \mathbf{I}_H$ can be neglected as compared to $\nabla_\perp \cdot \mathbf{I}_P$ in the evaluation of auroral field-aligned currents. Thus (3) can be approximated by

$$J_\parallel = -\nabla_\perp \cdot \mathbf{I}_P \qquad (4)$$

Equation (4) states that auroral field-aligned currents are associated with a divergence of height-integrated Pedersen currents. Generally, electric field changes contribute more to $\nabla_\perp \cdot \mathbf{I}_P$ than do Pedersen conductivity changes, so that we expect $J_\parallel$ to depend primarily on $\nabla \cdot \mathbf{E}$. In particular, $J_\parallel$ should be upward along the duskside convection reversal where $\nabla \cdot \mathbf{E} < 0$, and $J_\parallel$ should be downward along the morningside convection reversal where $\nabla \cdot \mathbf{E} > 0$. These field-aligned currents are commonly observed over the auroral zones from low-altitude satellites [e.g., *Iijima and Potemra*, 1976]. The regions of $\nabla \cdot \mathbf{E} \neq 0$ are indicated in Figure 6. The converging Pedersen currents on the duskside and diverging Pedersen currents on the dawnside, as well as the associated field-aligned currents, are illustrated in Figure 2. Discrete aurora are intense along the duskside convection reversal where $J_\parallel$ is upward.

Association Between Discrete Auroral Arcs and Field-Aligned Electric Fields

Upward field-aligned currents can be carried by electrons moving from the magnetosphere to the ionosphere, and it has been determined from rocket measurements over auroras [*McIlwain*, 1960; *Davis et al.*, 1960; *Evans*, 1967, 1968] that visible auroras result from the precipitation of ~1–10 keV electrons into the atmosphere. McIlwain concluded from his measurements over a bright arc that the electrons responsible for the arc were distributed over a rather narrow energy range. He referred to the energy distribution of these electrons as "monoenergetic" and suggested that the distribution may have been formed by electric field acceleration. This monoenergetic precipitation associated with discrete auroral features was found to be considerably different from that which McIlwain observed within a region of relatively low intensity diffuse auroral glow. The precipitation over the diffuse aurora was less intense than over the discrete auroral arcs, and the electrons were distributed over a wider range of energies. Such diffuse auroral precipitation can result from the direct precipitation of geomagnetically trapped electrons [see *Lyons and Williams*, 1984] without additional acceleration. Only the precipitation over the discrete arcs appeared to require acceleration by electric fields.

Later, measurements of the distribution of auroral arc electrons with pitch angle (angle between a particle's velocity and **B**) became available from satellites [*Hoffman and Evans*, 1968; *Holmgren et al.*, 1970; *Paschmann et al.*, 1972; *Mizera et al.*, 1976] and rockets [*O'Brien and Reasoner*, 1971; *Whalen and McDiarmid*, 1972; *Maehlum and Moestue*, 1973; *Arnoldy et al.*, 1974; *Lundin*, 1976]. These observations showed the distribution to occasionally be peaked in the downward direction along **B**, while being peaked in energy, and it was suggested that acceleration by electric fields aligned parallel to the auroral magnetic field lines could account for the observations. Figure 10 shows an example of the energy spectra within three pitch angle ranges obtained by *Arnoldy et al.* [1974] over an active auroral arc. Note the peak in the energy spectrum and the field alignment of the electrons at energies near 5 keV. (Field-aligned pitch angle distributions are not always seen over auroral arcs, however. This is because the distribution can become unstable to the generation of plasma waves. The waves perturb the electrons' velocities and drive their pitch angle distribution toward isotropy.)

The question of whether or not the electrons over arcs are accelerated by field-aligned electric fields became an important problem in auroral physics as a result of the electron precipitation measurements. A major difficulty with the idea was the existence of large numbers of electrons precipitating into the atmosphere at energies «1 keV. Such electrons can be seen in Figure 10 at energies between 30 and 200 eV. It was argued [*Westerlund*, 1969;

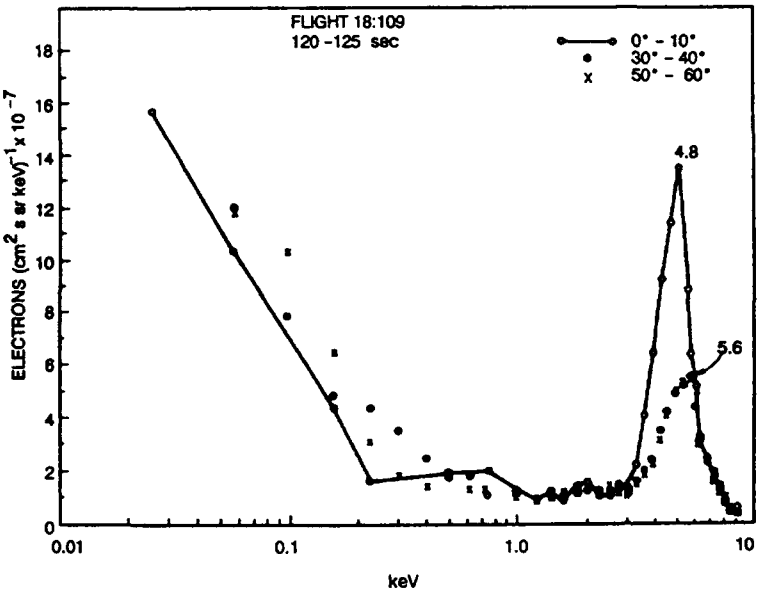

Figure 10. An example of the energy spectra of precipitating electrons obtained wthin three pitch angle ranges from a rocket above an auroral display [from *Arnoldy et al.*, 1974].

O'Brien, 1970] that a field-aligned electric field could not be responsible for the "monoenergetic" electrons at higher energies, since all electrons must be accelerated by the total field-aligned potential difference. Thus there should not be large numbers of precipitating, low-energy electrons.

A resolution to this difficulty was suggested by *Evans* [1974]. He noted that a field-aligned electric field that accelerates electrons downward toward the atmosphere will also act as a barrier to upgoing electrons. Thus upgoing electrons with an energy too low to surmount the total field-aligned potential difference will be reflected to appear as precipitating electrons. Evans also noted that the electrons that impinge upon the atmosphere after being accelerated by a field-aligned electric field will create a significant flux of low-energy secondary and backscattered electrons moving upwards out of the atmosphere. These electrons must be reflected back toward the atmosphere if the higher-energy electrons are accelerated by a field-aligned electric field, and Evans suggested that the reflected electrons could account for the large number of precipitating, low-energy electrons over arcs.

Model energy spectra of precipitating electrons at 0° and 45°, as calculated by *Evans* [1974], are shown in Figure 11. The total assumed field-aligned potential difference was 2 kV. The discontinuity in the calculated

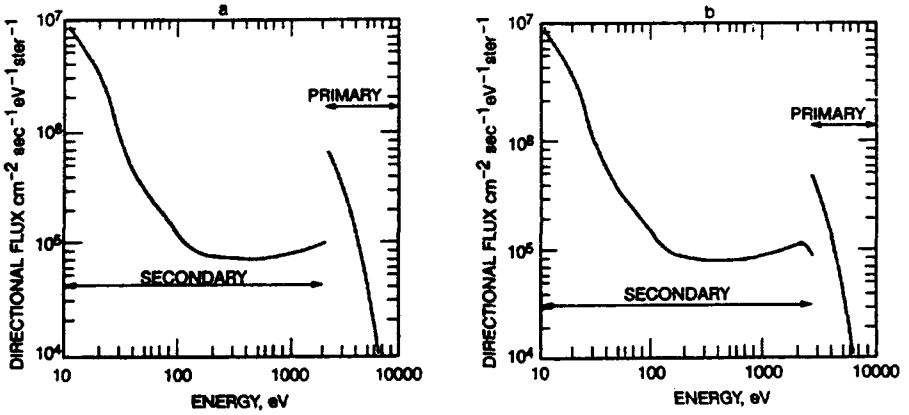

Figure 11. Model energy spectra of precipitating electrons at (*a*) 0° pitch angle and (*b*) 45° pitch angle. The electrons were assumed to have originated from an 800-eV plasma of density 1.5 cm^{-3} and were assumed to have been accelerated by a total field-aligned potential difference of 2 kV located at 2000 km altitude. The discontinuity in each of the spectra separates the primary auroral electrons of magnetospheric origin from the lower energy backscattered and secondary electrons of atmospheric origin [from *Evans*, 1974].

spectra near 2 keV clearly separates the accelerated auroral electrons of magnetospheric origin from the reflected lower-energy secondary and backscattered electrons of atmospheric origin. This discontinuity could not be discerned by a real particle detector, and it may well be smoothed by plasma wave-particle interactions. Nevertheless, the calculations reproduce the peak in the auroral energy spectra (at 2 keV in this case) and the enhanced fluxes of precipitating low-energy electrons. Evans found good agreement between his calculations and observations, thus providing important evidence that auroral arc electrons are accelerated by field-aligned electric fields.

Later, compelling evidence that auroral electrons are accelerated by field-aligned electric fields was obtained from S3-3 satellite observations over the auroral zones at ~5000–10,000 km altitude. *Shelly et al.* [1976] observed ionospheric ions streaming upward from the atmosphere, having been accelerated to energies of ~1 keV, and *Mizera and Fennell* [1977] observed ions having been accelerated upward along magnetic field lines simultaneously with electrons having been accelerated downward along the same field lines. Field-aligned electric fields are the only viable explanation so far presented for such observations.

Contour plots of simultaneously measured electron and ion distributions obtained at 7300 km altitude [*Mizera and Fennell*, 1977] are shown in Figure 12. The contours are drawn in the ($v_\perp$, $v_\parallel$) plane, where $v_\parallel$ is directed downward along **B** and $v_\perp$ is normal to **B**. The ion distribution can be seen to be strongly field aligned in the upgoing direction and to be peaked near $v_\parallel$ = 600 km/s, which corresponds to a proton energy of about 2 keV. The electron distribution in the downward direction can be seen to be peaked at $v_\parallel$ = 1.8×10^4 km/s (≈ 1 keV) between the two contours labeled. G. Mizera and Fennell made detailed comparisons between the particle distributions and features expected to result from acceleration by field-aligned electric fields. They found the distributions to be just what is expected if the satellite were located within a region of a field-aligned electric field having a total potential difference ~2 kV below the satellite and ~1 kV above the satellite. (The electron distribution is not field aligned near $v = 1.8 \times 10^4$ km/s because electrons have become trapped between the potential barrier above and the magnetic mirror below [see *Whipple*, 1977; *Chiu and Schulz*, 1978].)

The spatial association between discrete auroral arcs, the duskside convection reversal, and the boundary between open and closed magnetic field lines is shown in Figure 13 [*Lyons and de la Beaujardiere*, 1989]. This figure shows energy-time spectrograms of electrons (0.17–33 keV) and ions (0.09–3.9 keV/unit charge) versus universal time from the polar orbiting, spinning S3-3 satellite. The particle intensities are given by a grey scale in units of differential energy flux. In addition, the figure shows intensity-coded strips for 235-keV electrons and >80-keV ions, the electric potential along the satellite trajectory, and the pitch angle of the particles measured as the satellite spins.

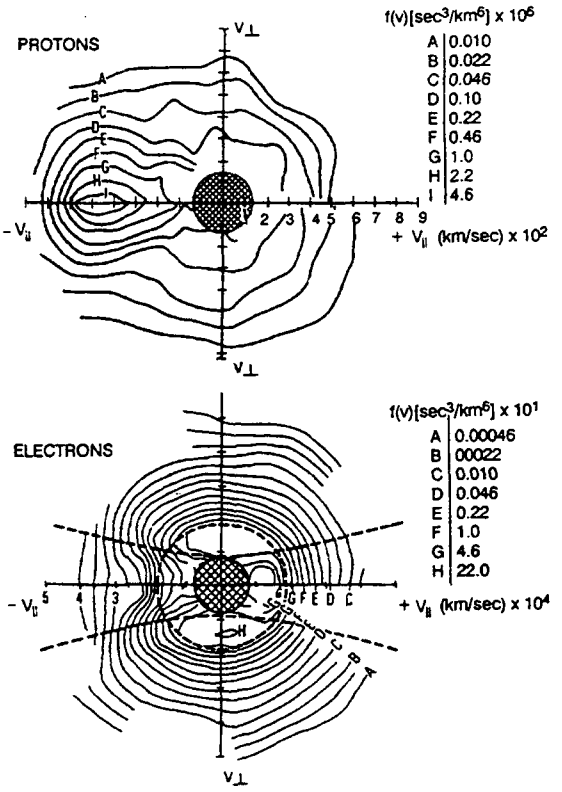

Figure 12. Contour plot in the ($v_\perp$, $v_\parallel$) plane of simultaneously measured electron and ion distributions from the S3-3 satellite at 7300 km altitude and ~1845 LT. These distributions indicate that the electrons were accelerated downward by a field-aligned potential difference of ~1 kV above the satellite and the ions were accelerated upward by a field-aligned potential difference of ~2 kV below the satellite. The dashed ellipse gives the boundary between accelerated magnetospheric electrons and electrons that cannot surmount the parallel potential difference above the satellite. The dashed hyperbola gives the boundary of the atmospheric loss cone [from *Mizera and Fennell*, 1977].

Detailed examination of data in the spectrogram reveals a discrete auroral arc (or arcs) just after 27,500 s UT. The arc is identified by enhanced fluxes of downgoing electrons at ~1 keV and enhanced fluxes of field-aligned (surrounding 180° pitch angle) upgoing ions. Comparison with the electric potential plot shows that the arc lies very near the minimum in the potential (i.e., at the duskside convection reversal). Enhanced fluxes of <600-eV electrons lie poleward of the auroral arc. These electrons are referred to as polar rain [*Winningham and Heikkila*, 1974]. They are the high-energy portion of the solar wind electron distribution that enters the magnetosphere along open, polar cap field lines. Equatorward of the arc, 235-keV electrons trapped on closed geomagnetic field lines can be identified by the minima at both 0° and 180°. These observations show that the arc and the convection reversal lie approximately at the open-closed field line boundary.

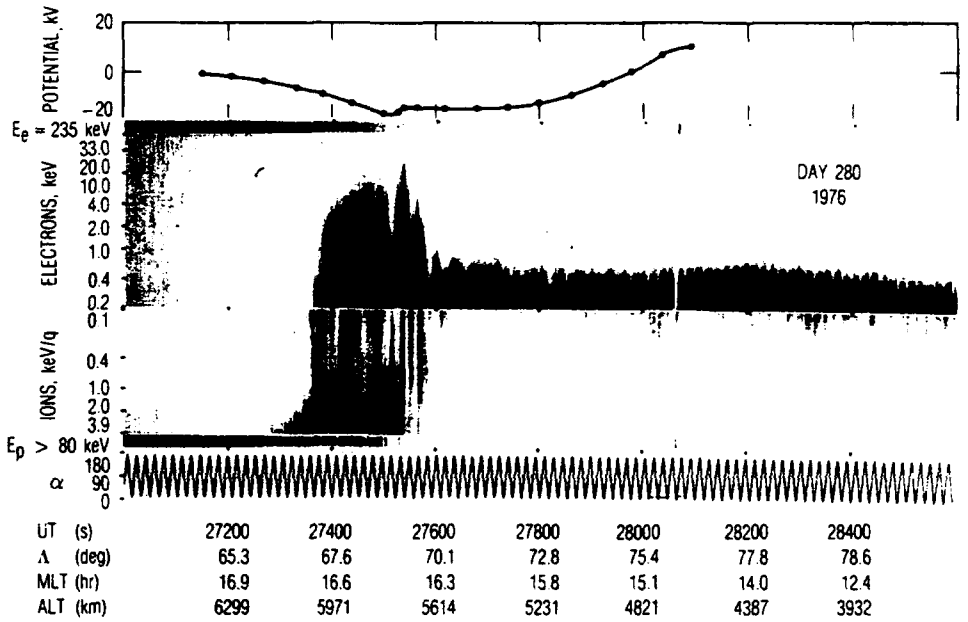

Figure 13. Spectrogram of S3-3 plasma data and plot of electric potential along satellite trajectory for 27,000 to 28,600 s UT on day 280, 1976. The center panels show the energy flux versus time for 0.2- to 33-keV electrons and for 0.1- to 3.9-keV/q ions. Energy flux levels are encoded in a grey scale with darker shading representing higher flux. Grey scale bands at the top and the bottom of the central spectrograms represent the intensities of 235-keV electrons and >80-keV protons, respectively. The pitch angle α of the particles samples is given by the jagged line below the particle data. Universal time, invariant magnetic latitude, magnetic local time, and satellite altitude are annotated along the bottom of the figure [from *Lyons and de la Beaujardiere*, 1989].

Field-Aligned Current-Voltage Relation

The foregoing discussion shows that discrete auroral arcs occur in regions of upward field-aligned currents, where $\nabla \cdot \mathbf{E} < 0$, and that they are formed by electrons accelerated by field-aligned electric fields. For a number of years, auroral field lines were viewed as "infinitely conducting," since there are essentially no collisions above the conducting portion of the ionosphere. As the collision frequency goes to zero, the collisional resistivity [*Spitzer*, 1962] goes to zero. Thus it was presumed that there could be no field-aligned potential difference $\Phi_{\parallel}$ unless there were some sort of additional resistivity. It was proposed [*Kindel and Kennel*, 1971; *Papadopoulos and Coffey*, 1974] that particle interactions with plasma waves driven unstable by auroral currents could lead to an anomalous resistivity. This additional resistivity could then allow for the existence of a significant $\Phi_{\parallel}$.

However, before appealing to anomalous resistivity, one should evaluate the maximum current density that can be carried along auroral field lines in the absence of additional resistivity. Field-aligned currents can be carried by ionospheric particles moving up to the magnetosphere and by magnetospheric particles precipitating into the ionosphere.

The maximum current that can be supplied by the ionospheric plasma is obtained by counting all particles of a given charge that have a component of velocity upward along the magnetic field and neglecting all particles with a downward velocity component. For a Maxwellian distribution of particles having charge q, mass m, density n, and thermal energy K_{th}, we obtain the maximum upgoing current density to be

$$J_{max} = nq(K_{th}/2\pi m)^{1/2} \qquad (5)$$

To evaluate J_{max}, we use the measurements of *Taylor et al.* [1975] and *Grebowsky et al.* [1976], which show that a density minimum, referred to as the high-latitude trough, lies in the vicinity of the convection reversal. Within this trough, O^+ is the dominant ion and $n \sim 10^9$–10^{10} m^{-3} near 1000 km altitude. Taking these parameters and $K_{th} = 0.172$ eV (2000° K), we obtain from (5) that $J_{max} = 6.5 \times 10^{-6}$ A/m^2 - 6.5×10^{-7} A/m^2 for upward currents carried by O^+ and $J_{max} = -(1.1 \times 10^{-5}$ A/m^2 -1.1×10^{-4} A/m^2) for downward currents carried by electrons.

Field-aligned currents in the auroral zones are often in the range 10^{-6} A/m^2 to a few times 10^{-5} A/m^2 [e.g., *Kamide and Rostoker*, 1977; *Anderson*, 1978; and references therein]. The downward currents can readily be supplied by upgoing ionospheric electrons; however, the upgoing currents cannot be supplied by ionospheric particles. We thus must consider the current from precipitating magnetospheric electrons to account for the upward field-aligned currents.

Magnetospheric particles are affected by the magnetic mirror force, which cause the particles' pitch angle α to vary with the magnetic field strength along a field line so as to conserve $\sin^2\alpha/B$ [see *Roederer*, 1970]. The pitch

angle of most particles reaches 90° before the particles reach the top of the atmosphere. Such particles bounce back and forth along magnetic field lines between the points where $\alpha = 90°$ and are trapped in the geomagnetic field. Particles with sufficiently small pitch angles reach the top of the atmosphere before α reaches 90°. Such particles are said to be in the loss cone, and they are absorbed into the atmosphere by collisions. Only particles within the loss cone can contribute to a field-aligned current, and auroral emissions result from the collisions of these particles with the atmosphere.

The loss cone is very small along auroral magnetic field lines, so that only a small fraction of the magnetospheric electrons can contribute to $J_\parallel$. However, a field-aligned potential difference that accelerates particles toward the atmosphere causes the particle $v_\parallel$ to increase, which causes their pitch angle to become more field aligned. This increases the number of particles in the loss cone. Thus the magnitude of $J_\parallel$ should increase with $\Phi_\parallel$. Assuming magnetospheric electrons have a Maxwellian energy distribution and an isotropic pitch angle distribution, the magnetic mirror force gives a relation between $J_\parallel$ and $\Phi_\parallel$ that can be written [*Knight*, 1973; *Lemaire and Scherer*, 1974; *Antonova and Tverskoy*, 1975]:

$$J_\parallel = en(K_{th}/2\pi m_e)^{1/2} R\{1 - (1 - R^{-1}) \exp[-e\Phi_\parallel/K_{th}(R - 1)]\} \quad (6)$$

Here $R = B_i/B_{\Phi\parallel}$ is the ratio between the magnetic field B_i in the ionosphere and the magnetic field $B_{\Phi\parallel}$ at the top of the field-aligned potential variation. Relation (6) is independent of the distribution of the potential along field lines, except for the assumption that no particles that are incident upon the top of the field-aligned potential variation attain 90° pitch angle before falling through the entire potential variation. This is not a significant restriction for the purposes here.

Figure 14 shows $J_\parallel$ versus $\Phi_\parallel$ as obtained from (6) for $n = 1$ cm^{-3} and $K_{th} = 1$ keV and various values of R. Values of $J_\parallel$ and $\Phi_\parallel$ for other values of n and K_{th} can easily be obtained using the normalizations indicated along the axes of the figure. The value $n = 1$ cm^{-3} is reasonable for auroral field lines, whereas K_{th} is closer to a few hundred electron volts. The potential variation generally occurs between about 5000 and 10,000 km altitude [*Gorney et al.*, 1981], so that $R = 30$ should be typical. From Figure 14 we see that $J_\parallel$ cannot exceed $\sim 5 \times 10^{-7}$ A/m^2 with $\Phi_\parallel = 0$.

This shows that the upward field-aligned currents associated with auroral arcs (which are typically 10^{-6} A/m^2 to a few times 10^{-5} A/m^2) cannot be supplied by the collisionless plasma along auroral field lines with $\Phi_\parallel = 0$. However, these currents can be supplied if $\Phi_\parallel \sim 1$–10 kV. Thus the upward field-aligned currents observed over auroral arcs require the observed values of $\Phi_\parallel$! No additional resistivity is required.

We can test the consistency of (6) over auroral arcs by noting from Figure 14 that $J_\parallel \propto \Phi_\parallel$ for $e\Phi_\parallel/K_{th} \sim 3$–30 kV. This corresponds to $\Phi_\parallel \sim 1$–10 kV, which are typical values for arcs. From (6) we obtain that for $1 \ll e\Phi_\parallel/K_{th} \ll R$:

$$J_\parallel = K\Phi_\parallel \quad (7)$$

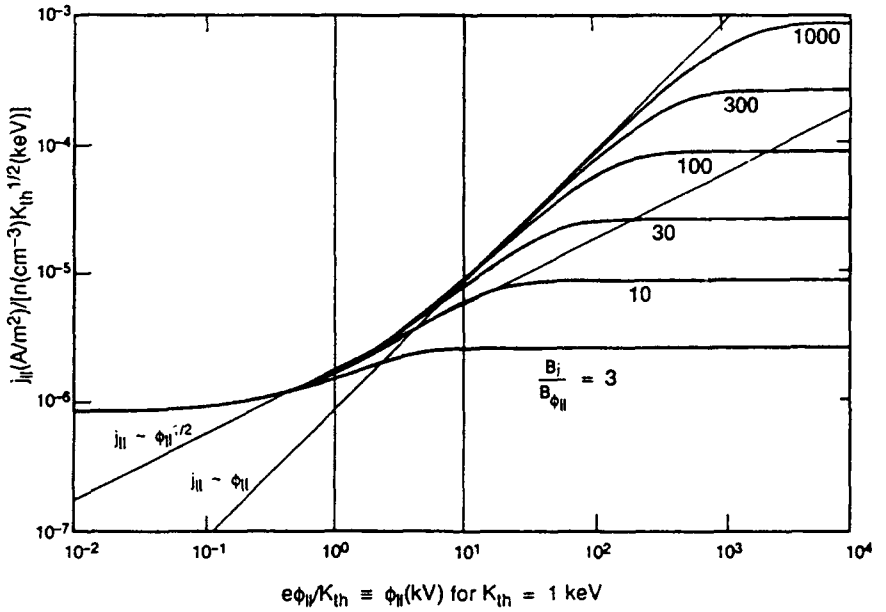

Figure 14. The $j_\parallel$ versus $\Phi_\parallel$ relation for single-particle motion along field lines for a magnetospheric electron population with density $n = 1$ cm^{-3} and a thermal energy $K_{th} = 1$ keV for various values of $R = B_i/B_{\Phi\parallel}$. Values for other values of n and K_{th} can be obtained from the normalizations given along the axes. Lines corresponding to $j_\parallel \propto \Phi_\parallel^{1/2}$ and $j_\parallel \propto \Phi_\parallel^1$ and to $e\Phi_\parallel/K_{th} = 1$ and 10 are shown for reference [from *Lyons*, 1981*b*].

where $K = e^2 n/(2\pi m_e K_{th})^{1/2}$. It is difficult to measure the detailed spatial variation of $J_\parallel$ over arcs, but it is relatively easy to measure the variation of the total precipitating electron energy flux ε_p. We can write ε_p as the sum of the energy flux ε_{p0} that would be carried by the electrons for $\Phi_\parallel = 0$ and the amount $\Phi_\parallel J_\parallel$ gained from the electrons falling through $\Phi_\parallel$. Over arcs, we typically have $K_{th} \ll e\Phi_\parallel$, so that $\varepsilon_{p0} \ll \Phi_\parallel J_\parallel$, and we may approximate ε_p by

$$\varepsilon_p \approx \Phi_\parallel J_\parallel = K\Phi_\parallel^2 \tag{8}$$

A test of (8) is shown in Figure 15 [from *Lyons et al.*, 1979] using observations of precipitating electrons obtained from the Polar 3 rocket [*Maynard et al.*, 1977; *Evans et al.*, 1977]. The rocket was launched toward the north. It flew over a broad auroral arc between about 150 and 210 km down range and it reentered the atmosphere at a distance of about 400 km within a weak arc. The energy spectra of the electrons were obtained along the rocket trajectory. From these spectra, ε_p was obtained from integrating over energy and $\Phi_\parallel$ was estimated from the peak in the electron energy spectra.

In Figure 15 the solid line gives the measured values of ε_p and the dots give $K\Phi_\parallel^2$. Two values of K were used, the higher value (4.7×10^{-4} J/m^2 s kV^2) giving a good fit to ε_p before 220 km and the lower value (1×10^{-4} J/m^2 s kV^2) giving a good fit after 220 km. It is evident from this figure that relation (8) held throughout the entire flight, except near 220 km where n or K_{th} may have changed. This relation has also been verified using DE satellite measurements over auroras [*Weimer et al.*, 1985, 1987; *Lu et al.*, 1991]. These tests demonstrate that (6) correctly gives the relation between $J_\parallel$ and $\Phi_\parallel$ over auroral arcs. However, this by itself does not explain why $J_\parallel$'s over auroral arcs are sufficiently large that $\Phi_\parallel > 0$ is required.

Why Field-Aligned Electric Fields Are Required

It has been well established from observations that auroral arcs are associated with changes in the ionospheric electric fields having $\nabla \cdot E < 0$, such as occur along the duskside convection reversal [*Frank and Gurnett*, 1971; *Gurnett and Frank*, 1973; *Swift and Gurnett*, 1973; *Maynard et al.*, 1977; *Heelis et al.*, 1981; *Burke*, 1981; *Temerin et al.*, 1981]. To describe why such an electric field structure leads to auroral arcs having $\Phi_\parallel > 0$, we first idealize the magnetospheric convection reversal as a discontinuity in the electric field at altitudes above all field-aligned potential differences. The solid line in Figure 16 illustrates the potential Φ from such a field plotted as a function of distance x_i as mapped to the ionosphere. The electric field is taken to be uniform except for the discontinuity at $x_i = 0$. Given this high-altitude potential distribution, we would like to calculate the ionospheric potential Φ_i versus x_i as illustrated by the dashed line in Figure 16.

From the requirement for current continuity in the ionosphere, equation (4), we have

$$J_\parallel = \partial/\partial x_i [\Sigma_p (\partial\Phi_i/\partial x_i)] \tag{9}$$

Equation (9) can be used to solve for the ionospheric potential $\Phi_i(x_i)$ for a specified high-altitude potential distribution $\Phi(x_i)$ if $J_\parallel$ and Σ_p are written as a function of $\Phi_\parallel = (\Phi_i - \Phi)$. Equation (6) gives $J_\parallel$ as a function of $\Phi_\parallel$. Also, Σ_p can be written as a function of ε_p [*Harel et al.*,

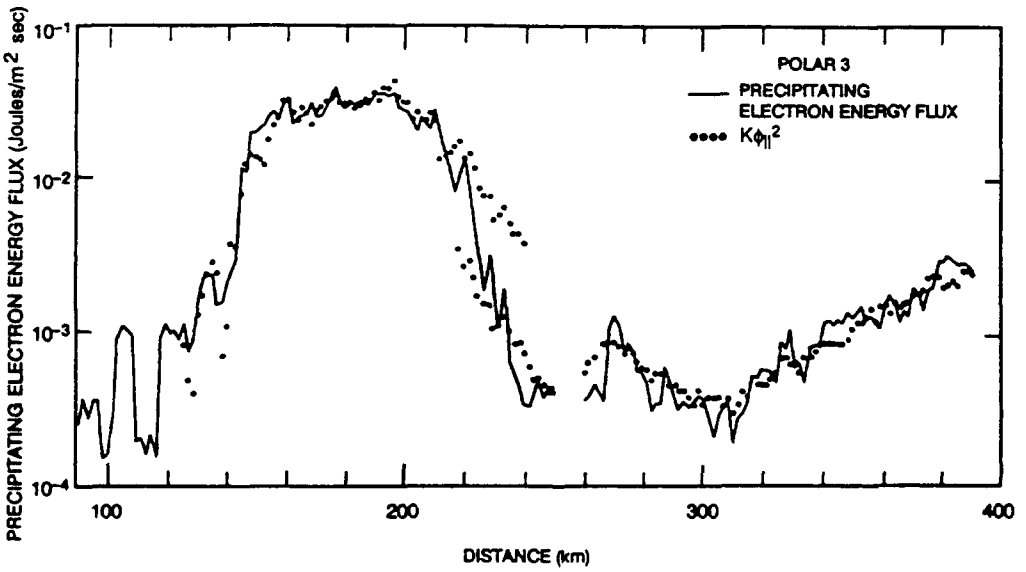

Figure 15. Precipitating electron energy flux and the functional form $K\Phi_\parallel^2$ versus horizontal distance (approximately to the north) along the Polar 3 rocket [*Maynard et al.*, 1977; *Evans et al.*, 1977] trajectory. Values of $K\Phi_\parallel^2$ are shown from 120 km to the end of the flight, where $\Phi_\parallel$'s > 1 kV were inferred from peaks in the energy spectra of precipitating electrons. Two values of K were used, the higher value (4.7×10^{-4} j/m^2 s kV^2) giving a good fit before 220 km and the lower value (1×10^{-4} j/m^2 s kV^2) giving a good fit after 220 km [from *Lyons et al.*, 1979].

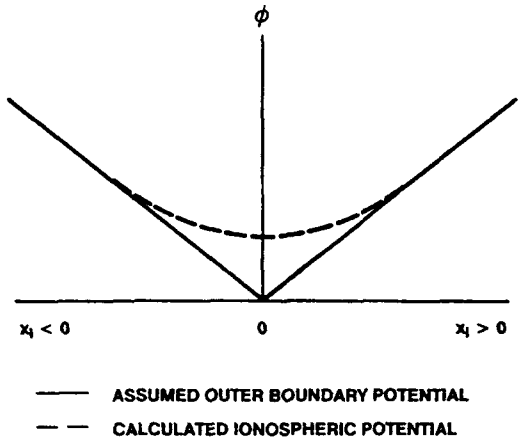

Figure 16. Electric potential as a function of distance as mapped along magnetic field lines to the ionosphere. The solid line gives the magnetospheric potential above all field-aligned potential differences for a convection reversal idealized as a discontinuity in the electric field. The dashed line gives the ionospheric potential [from *Lyons*, 1980].

1981], which can be written as a function of $\Phi_{\parallel}$ [*Lundin and Sandahl*, 1978]. This allows (9) to be written as a second-order differential equation that can readily be solved numerically for $\Phi_i(x_i)$ [see *Lyons*, 1980, 1981*b*]. However, if we let Σ_p be constant, use (7), and use the model for $\Phi(x_i)$ shown in Figure 16, (9) can be written as an equation that can be solved analytically:

$$\frac{d^2\Phi_i}{dx_i^2} = \frac{K}{\Sigma_p}\left[\Phi_i + \begin{Bmatrix} E_1 \\ E_2 \end{Bmatrix} x_i\right] \qquad (10)$$

Here the high-altitude electric field, as mapped along field lines to the ionosphere, is E_2 for $x_i > 0$ and E_1 for $x_i < 0$.

The solution to (10) under the boundary conditions that Φ_i is continuous at $x_i = 0$ and that $\Phi_{\parallel} \rightarrow 0$ as $x_i \rightarrow \pm\infty$ is

$$\Phi_{\parallel} = \Phi_{\parallel 0} \exp(-|x_i|/x_W),$$

where the half width

$$x_W = (\Sigma_p/K)^{1/2} = (\Sigma_p/e^2N)^{1/2}(2\pi m_e K_{th})^{1/4}$$

and the maximum field-aligned potential difference is

$$\Phi_{\parallel 0} = (x_w/2)(E_1 - E_2).$$

Taking $\Sigma_p = 5$ mhos, $n = 10^{-6}$ m^{-3}, and $K_{th} = 0.25$ kV, we obtain $x_W = 54$ km. This is a natural half width for auroral acceleration regions. Taking $E_1 - E_2 = 0.1$ mV/m, which is typical for the evening convection reversal, we obtain $\Phi_{\parallel 0} = 2.5$ kV. This analytical result demonstrates that field-aligned potential differences of a few kilovolts are necessary for the maintenance of current continuity in the ionosphere in the vicinity of the duskside convection reversal.

While a total width of ~100 km is reasonable for regions of auroral arcs, individual arcs are generally significantly narrower. This is because the high-altitude electric field distribution is generally significantly more complex than in the idealized model just described. However, (9) can also be used to model the more realistic situation, though the solution must be obtained numerically.

The high-altitude potential distribution inferred as a function of ionospheric distance from the Polar 3 rocket data is shown by the jagged, solid line in Figure 17. This distribution was obtained from subtracting $\Phi_{\parallel}$, as obtained from the peak in the energy spectra of precipitating electrons, from the electric potential measured along the rocket trajectory (smooth solid line). The high-altitude potential distribution shows a large electric field change

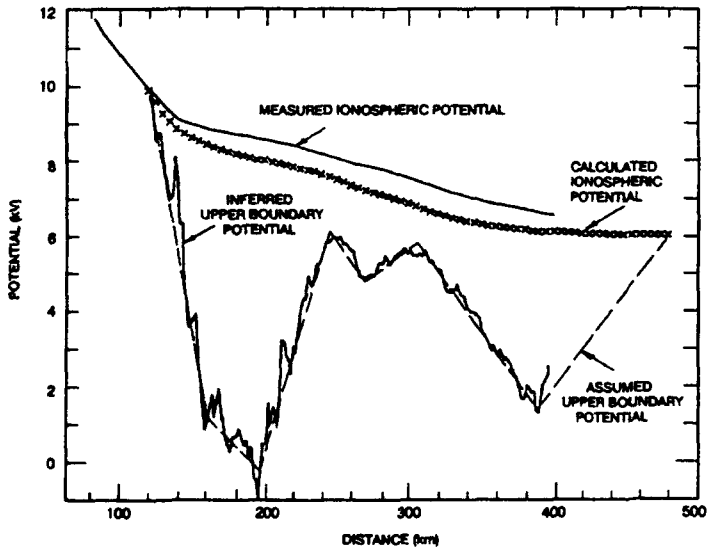

Figure 17. Measured ionospheric potential from the Polar 3 rocket, inferred and assumed potential above all field-aligned potential differences, and ionospheric potential calculated by solving the current continuity equation in the ionosphere, all plotted as a function of horizontal distance (approximately to the north) along the rocket trajectory.

(several hundred millivolts per meter) with $\nabla \cdot \mathbf{E} < 0$ over the intense arc and a weaker electric field change with $\nabla \cdot \mathbf{E} < 0$ over the weaker arc to the north.

Equation (9) was solved numerically by *Lyons* [1981*a*] for $\Phi_i(x_i)$ using the dashed line in Figure 17 for $\Phi(x_i)$. The calculated ionospheric potential distribution is given by the crosses in the figure, and the results agree with the measure potential to within ~0.5 kV. This shows the field-aligned potential differences that accelerate electrons over auroral arcs can be understood in terms of the magnetospheric electric field distribution, the $J_\parallel$ versus $\Phi_\parallel$ relation (6), and the requirement for current continuity in the ionosphere. Also, we know why an electric field reversal having $\nabla \cdot \mathbf{E} < 0$ exists along the duskside convection reversal. However, we do not yet understand why complex electric field distributions, such as shown in Figure 17, develop in the magnetosphere.

4. EFFECTS OF NEUTRAL WINDS IN CONDUCTING REGION

As in the above analysis, auroral electrodynamics is usually studied under the assumption that the neutral wind velocity $\mathbf{V}_n$ within the conducting altitudes of the ionosphere can be neglected. While this neglect is generally valid, there are situations where the winds may have interesting effects.

The relations between electric fields and currents in the ionosphere are valid in the frame of reference of the neutrals. The electric field in the neutral frame $\mathbf{E}'$ is related to the electric field $\mathbf{E}$ in the stationary frame by

$$\mathbf{E}' = \mathbf{E} + \mathbf{V}_n \times \mathbf{B}$$

Assuming that $\mathbf{V}_n$ is approximately constant with height over the conducting region (~120–150 km) of the ionosphere (or is an appropriately weighted average value), we may write the height-integrated Pedersen current as

$$\mathbf{I}_p = \Sigma_p \mathbf{E}' = \Sigma_p (-\mathbf{V}_E + \mathbf{V}_n) \times \mathbf{B}, \qquad (11)$$

where the electric field drift speed

$$\mathbf{V}_E = (\mathbf{E} \times \mathbf{B})/B^2.$$

Measurements of $\mathbf{V}_n$ at the conducting altitudes are limited; however, modeling results show that wind speeds in polar regions should generally be about 100 m/s [e.g., *Roble et al.*, 1984]. This speed corresponds to an electric field magnitude of 5 mV/m, which is significantly less than typical auroral electric fields. Such winds may drive observable large-scale currents over the polar caps [*Lyons et al.*, 1985] that are much weaker than auroral currents, but winds of this magnitude can generally be neglected in (11) when studying auroral electrodynamics.

However, ionospheric electric fields accelerate neutrals as a result of collisions between the neutral and ions, and this acceleration is enhanced in the conducting region within auroras. The enhancement results from increased ionospheric densities caused by the auroral particle precipitation. Such acceleration has the potential for modifying $\mathbf{I}_p$ and thus affecting $J_\parallel$ and the electrodynamics of auroras.

With the neutral winds, and taking Σ_p to be constant, we have that

$$J_\parallel = -\nabla_\perp \cdot \Sigma_p \mathbf{E}' = \Sigma_p [\nabla_\perp \cdot \mathbf{E} + \mathbf{B} \cdot \nabla \times \mathbf{V}_n] \qquad (12)$$

As in (4), a negligible $\nabla \times \mathbf{B}$ term has been dropped from (12). This equation shows the $\nabla \times \mathbf{V}_n$, as well as $\nabla_\perp \cdot \mathbf{E}$, can drive field-aligned currents.

Within discrete auroral arcs the ionospheric electric field is significantly less than the ionospheric mapping of the magnetospheric electric field, as can be seen in Figures 16 and 17. This reduces the wind acceleration within such arcs. Within diffuse auroras, however, $\Phi_\parallel = 0$, so that the magnetospheric electric field maps to the ionosphere without being reduced. Since ionospheric densities are significantly enhanced as a result of the electron precipitation within diffuse auroras (though not as much as within discrete auroras), acceleration of $\mathbf{V}_n$ should be particularly strong within diffuse auroras. Such acceleration should be strongest on the dawnside where the diffuse auroras are most intense and can be very stable.

Lyons and Walterscheid [1985] and *Walterscheid and Lyons* [1989] have simulated the neutral response to intense postmidnight diffuse auroras and found that winds in the conducting region of the ionosphere could reach up to several hundred meters per second. These strong winds were referred to as "jet." An example of their results after 2 hours of simulated time are shown in Figure 18. The diffuse aurora was centered at 0 km north-south distance

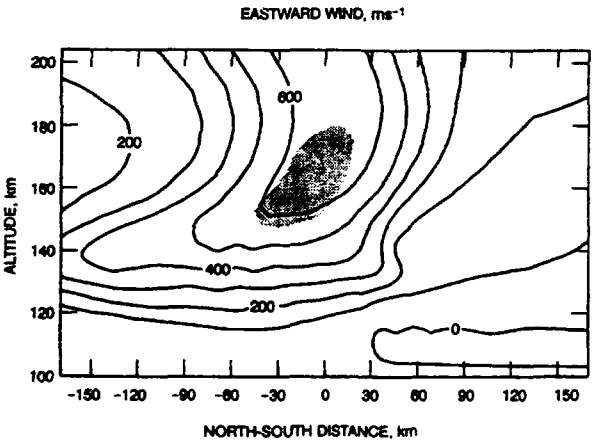

Figure 18. Simulated eastward directed winds along a diffuse aurora having a peak precipitating electron energy flux of 7.6 ergs/cm^2 s over a 50-km latitudinal width centered at 0 km. Results shown are after 2 hours of simulated time, and the shaded area is where the wind speed exceeded the local sound speed [from *Walterscheid and Lyons*, 1989].

and had a peak precipitating electron energy flux of 7.6 ergs/cm^2 s. Peak winds can be seen to be 200 m/s at 120 km altitude, increasing to over 600 km/s above 150 km. Such winds, if they are found to exist, would be a dramatic result of magnetosphere-ionosphere coupling.

Neutral winds accelerated within discrete arcs, while expected to be less intense than within diffuse auroras, have the potential for reducing $|\nabla_\perp \cdot \Sigma_P \mathbf{E}|$ and thus reducing the intensity of arcs. Assuming uniformity in the east-west direction and letting x_i be in the south-to-north direction, (12) becomes

$$J_\parallel = \partial/\partial x_i [\Sigma_p (\partial \Phi_i/\partial x_i) - UB], \quad (13)$$

where U is the eastward component of the neutral wind that is representative of the conducting portion of the ionosphere. This equation is identical to (9) except for the addition of the neutral wind term. However, the neutral winds increase with time as a result of ion-neutral collisions. Thus (9) describes a feedback between neutral winds and auroral arc electrodynamics.

The wind acceleration depends upon the ionospheric electric field and densities and can be written in terms of the height-integrated Pedersen current as [*Richmond and Matsushita*, 1975]:

$$\partial U/\partial t = I_p B/(\rho \Delta z), \quad (14)$$

where ρ is the neutral density. The quantity Δz is the effective thickness of the conducting portion of the ionosphere defined so that $\Sigma_p = \sigma_p \Delta z$, where σ_P is a representative Pedersen conductivity.

Assuming a magnetospheric electric field of the type illustrated in Figure 16 turns on at $t = 0$ with $U = 0$, (13) and (14) were solved numerically by *Lyons and Walterscheid* [1986] for $\Phi_i(x_i)$ and $U(x_i)$ as a function of time. Results are shown in Figure 19. Notice that U increases approximately linearly with time. While such acceleration might be expected to reduce I_p, and thus the intensity of the arc, the plots of V_E, $J_\parallel$, and ε_p in Figure 19 show that the intensity of the arc is reduced very little by the wind acceleration.

The maintenance of the arc intensity is a result of a negative feedback that occurs between the winds and the arc electrodynamics. As U increases, $(\partial/\partial x_i)V_P$ decreases. This decreases $J_\parallel$. However, the decrease in $J_\parallel$ is associated with a decrease in $\Phi_\parallel$, which increases the ionospheric electric field. The increase in $|\partial\Phi_i/\partial x_i|$ with time can be seen in the upper panels of Figure 19. The increase in the electric field acts to maintain the intensity of the arc in the presence of the accelerating neutral winds. This negative feedback also keeps the drag on the neutrals by the ions approximately constant as the winds increase, which enhances the acceleration of the neutrals.

5. SUMMARY

Discrete auroral arcs result from the existence of a magnetospheric electric field and a conducting ionosphere. This tutorial has concentrated on the basic processes responsible for the arcs and is most directly applicable to large-scale, time-stationary, arcs that lie near the boundary

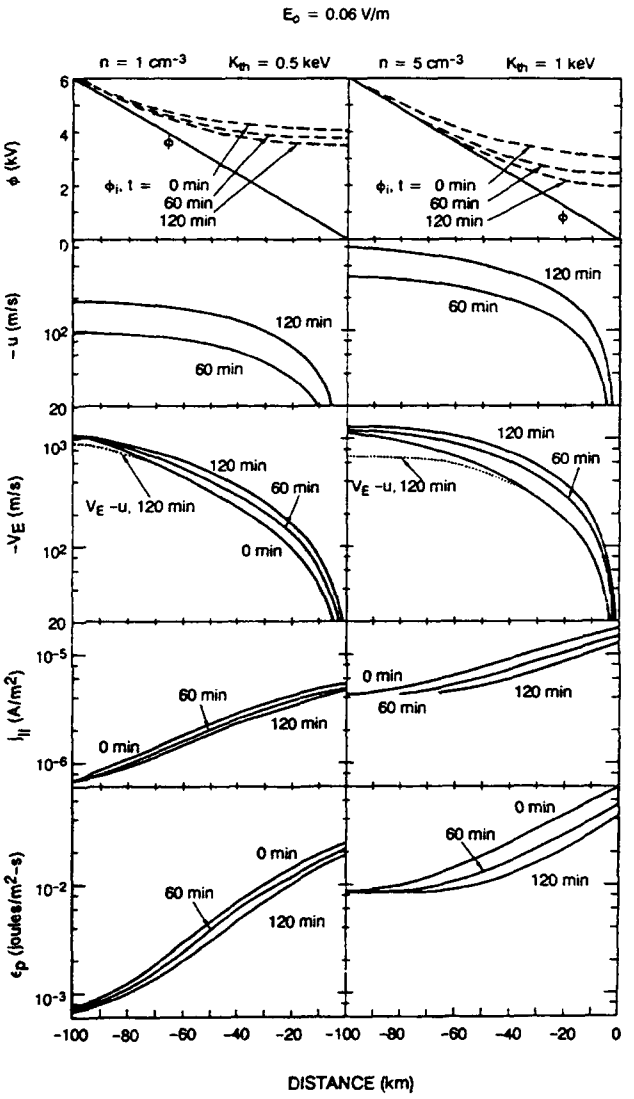

Figure 19. Numerical solution to the ionospheric current continuity equation and the neutral momentum equation for a magnetospheric potential distribution of the form shown in Figure 16 having an electric field magnitude as mapped to the ionosphere of 0.6 mV/m. Distance is in the ionosphere, and only $x_i \leq 0$ is shown since results are symmetric about $x_i = 0$. The density and thermal energy of the magnetospheric electron population are different for the two columns, as indicated at the top of each column. The top panels show the assumed magnetospheric potential (solid line) and the calculated ionospheric potentials (dashed lines) for $t = 0$, 60, and 120 min following the onset of neutral wind acceleration. The other panels from top to bottom, respectively, show the neutral wind speed ($-U$ is plotted, since the winds are westward), the electric field drift speed ($-V_E$), the upward field-aligned current density, and the precipitating electron energy flux [from *Lyons and Walterscheid*, 1986].

between open and closed field lines. Additional important processes give rise to the complex structure and dynamics often seen in auroral arcs. Such processes and relevant references are contained in the review by *Lysak* [1990].

The connection of the interplanetary and geomagnetic fields allows the interplanetary electric field to be transmitted to the Earth's magnetosphere. The electric field maps directly to the polar caps along open field lines. This polar cap electric field is associated with charges along the boundary between open and closed magnetic field lines, and these charges extend the electric field to the closed field line region of the magnetosphere.

Charging of the boundary between open and closed field lines requires that an electric field be directed along the boundary. This electric field, known as the reconnection electric field, maps to a magnetic x line at the magnetopause that extends around the entire magnetosphere. The critical assumption of ideal magnetohydrodynamics, $\mathbf{E} = -\mathbf{V} \times \mathbf{B}$, cannot be valid along this x line. However, gyroviscosity that results from the gradient of the off-diagonal elements of the electron pressure tensor is sufficient to balance the force from the reconnection electric field at the x line. Additional resistivity, such as anomalous resistivity from wave-particle interactions, is not required for there to be a finite reconnection electric field.

The mapping of the magnetospheric electric field to the ionosphere gives an electric field reversal in the auroral zones lying near the ionospheric mapping of the open-closed field line boundary. This electric field reversal drives ionospheric currents having $\nabla \cdot \mathbf{I}_P \neq 0$, which leads to magnetic field-aligned currents in order to maintain current continuity. The field-aligned currents are downward along the dawnside electric field reversal and upward along the duskside reversal. The downward currents can be carried by upgoing ionospheric electrons; however, the upgoing currents densities are too large to be carried with a field-aligned potential difference $\Phi_{\parallel} = 0$. As a result, a field-aligned potential difference forms having a typical magnitude of 1–10 kV. This field-aligned potential difference is required to maintain ionospheric current continuity, and it accelerates magnetospheric electrons downward toward the atmosphere. The accelerated electrons impinge upon the atmosphere leading to discrete auroral arcs. As is the case with the reconnection electric field, anomalous resistivity is not required to maintain a $\Phi_{\parallel} > 0$.

The electric fields and enhanced electron densities in the auroral ionosphere lead to enhanced interactions with neutral atmospheric constituents. In particular, collisions with ions accelerate the neutrals and may lead to winds that are significantly larger than those that are typically of the conducting altitude region of the ionosphere. The winds are predicted to become particularly strong within postmidnight diffuse auroras. These winds can affect ionospheric currents, but it does not appear likely that they will have significant effects on the electrodynamics of discrete auroral arcs.

ACKNOWLEDGMENTS. This paper is based on a tutorial which I gave at the CEDAR meeting in Boulder in June 1990. I thank the organizers of that meeting for inviting me to give the tutorial and for arranging for its publication in *Reviews of Geophysics*. I greatly appreciate the helpful comments from both referees and from the editor-in-chief. The work has been supported by NASA grant NAGW-2126 (Space Physics Theory Program), NSF grant ATM-8800602, and the Aerospace Sponsored Research Program.

M. Neugebauer was the editor responsible for this paper. She thanks Lawrence Zanetti for his assistance in evaluating its technical content and Deborah Hutchinson for serving as a cross-disciplinary referee.

REFERENCES

Akasofu, S.-I., *Physics of Magnetospheric Substorms*, D. Reidel, Hingham, Mass., 1977.

Anderson, H. R., Birkeland currents and auroral structure, *J. Geomagn. Geoelectr., 30*, 381, 1978.

Anger, C. D., et al., Scientific results from the Viking imager: An introduction, *Geophys. Res. Lett., 14*, 383, 1987.

Antonova, E. E., and B. A. Tverskoy, Nature of the electron precipitation band of the "inverted V" type and the Harang discontinuity in the evening sector of the auroral ionosphere, *Geomagn. Aeron., 15*, 85, 1975.

Arnoldy, R. L., P. B. Lewis, and P. O. Isaacson, Field-aligned auroral electron fluxes, *J. Geophys. Res., 79*, 4208, 1974.

Burke, W. J., Electric fields, Birkeland currents, and electron precipitation in the vicinity of discrete auroral arcs, in *Physics of Auroral Arc Formation, Geophys. Monogr. Ser.*, vol. 25, edited by S.-I. Akasofu and J. R. Kan, p. 169, AGU, Washington, D. C., 1981.

Burke, W. J., M. C. Kelly, R. C. Sagalyn, M. Smiddy, and S. T. Lai, Polar cap electric field structures with a northward interplanetary magnetic field, *Geophys. Res. Lett., 6*, 2431, 1979.

Burkhart, G. R., J. F. Drake, and J. Chen, Magnetic Reconnection in collisionless plasmas: Prescribed fields, *J. Geophys. Res., 92*, 18,833, 1990.

Caufman, D. P., and D. A. Gurnett, Double-probe measurements of convection electric fields with the Injun 5 satellite, *J. Geophys. Res., 76*, 6014, 1971.

Chiu, Y. T., and M. Schulz, Self-consistent particle and parallel electrostatic field distributions in the magnetospheric-ionospheric auroral regions, *J. Geophys. Res., 83*, 629, 1978.

Coroniti, F. V., Explosive tail reconnection: The growth and expansion phase of magnetospheric substorms, *J. Geophys. Res., 80*, 7427, 1985.

Crooker, N. U., Dayside merging and cusp geometry, *J. Geophys. Res., 84*, 951, 1979.

Davis, L. R., O. E. Berg, and L. H. Meridith, Direct measurements of particle fluxes in and near auroras, in *Space Res., I*, p. 721, North-Holland, New York, 1960.

Davis, T. N., The morphology of the polar aurora, *J. Geophys. Res., 65*, 3497, 1960.

Davis, T. N., The morphology of the auroral displays of 1957–1958, 2, Detail analysis of Alaska data and analyses of high-latitude data, *J. Geophys. Res., 67*, 75, 1962.

de la Beaujardiere, O., V. B. Wickwar, J. D. Kelly, and J. H. King, IMF-B_y effects on the high-latitude night side convection, *Geophys. Res. Lett., 12*, 461, 1985.

Dungey, J. W., Noise-free neutral sheets, Proceedings of an International Workshop in Space Plasma, Potsdam, Germany, *Eur. Space Agency Spec. Publ., ESA SP-285*, 15, 1988.

Evans, D. S., A 10-cps periodicity in the precipitation of auroral zone electrons, *J. Geophys. Res., 72*, 4281, 1967.

Evans, D. S., The observations of a near monoenergetic flux of auroral electrons, *J. Geophys. Res., 73*, 2315, 1968.

Evans, D. S., Precipitating electrons formed by a magnetic field-aligned potential difference, *J. Geophys. Res., 79,* 2853, 1974.

Evans, D. S., N. C. Maynard, J. Troim, T. Jacobsen, and A. Egeland, Auroral arc electric field and particle comparisons, 2, Electrodynamics of an arc, *J. Geophys. Res., 82,* 2235, 1977.

Feldstein, Y. I., Some problems concerning the morphology of auroras and disturbances at high latitudes, *Geomagn. Aeron., 3,* 183, 1963.

Foster, J. C., An empirical electric field model derived from Chatanika radar data, *J. Geophys. Res., 88,* 981, 1983.

Foster, J. C., J. M. Holt, R. G. Musgrove, and D. S. Evans, Solar wind dependencies of high-latitude convection and precipitation, in *Solar Wind-Magnetosphere Coupling,* edited by Y. Kamide and J. A. Slavin, p. 477, Terra Scientific, Tokyo, 1986.

Frank, L. A., and J. D. Craven, Imaging results from Dynamics Explorer 1, *Rev. Geophys., 26,* 249, 1988.

Frank, L. A., and D. A. Gurnett, Distributions of plasmas and electric fields over the auroral zones and polar caps, *J. Geophys. Res., 76,* 6829, 1971.

Gorney, D. J., A. Clarke, D. Croley, J. Fennell, J. Luhmann, and P. Mizera, The distribution of ion beams and conics below 8000 km, *J. Geophys. Res., 86,* 83, 1981.

Grebowsky, J. M., A. J. Chen, and H. A. Taylor, Jr., High latitude troughs and the polar cap boundary, *J. Geophys. Res., 81,* 690, 1976.

Gurnett, D. A., and L. A. Frank, Observed relationships between electric fields and auroral particle precipitation, *J. Geophys. Res., 78,* 145, 1973.

Harel, M., R. A. Wolf, P. H. Reiff, and R. W. Spiro, Quantitative simulation of a magnetospheric substorm, 1, Model logic and overview, *J. Geophys. Res., 86,* 2217, 1981.

Heelis, R. A., The effects of interplanetary magnetic field orientation on day side high-latitude convection, *J. Geophys. Res., 89,* 2873, 1984.

Heelis, R. A., Studies of ionospheric plasma and electrodynamics and their application to ionosphere-magnetosphere coupling, *Rev. Geophys., 26,* 317, 1988.

Heelis, R. A., W. B. Hanson, and J. L. Burch, AE-C observations of electric fields around auroral arcs, in *Physics of Auroral Arc Formation, Geophys. Monogr. Ser.,* vol. 25, edited by S.-I. Akasofu and J. R. Kan, p. 154, AGU, Washington, D. C., 1981.

Heelis, R. A., J. C. Foster, O. de la Beaujardiere, and J. Holt, Multistation measurements of high-latitude ionospheric convection, *J. Geophys. Res., 88,* 10,111, 1983.

Heikkila, W. J., Impulsive penetration and viscous interaction, Proceedings of Magnetospheric Boundary Layer Conference, *Eur. Space Agency Spec. Publ., ESA SP-148,* 375, 1979.

Heppner, J. P., Electric fields in the magnetosphere, in *Critical Problems of Magnetospheric Physics,* edited by E. R. Dyer, p. 107, IUCSTP Secretariat, National Academy of Sciences, Washington, D. C., 1972.

Heppner, J. P., and N. C. Maynard, Empirical high-latitude electric field models, *J. Geophys. Res., 92,* 4467, 1987.

Hoffman, R. A., and D. S. Evans, Field-aligned electron bursts at high-latitudes observed by OGO 4, *J. Geophys. Res., 73,* 6201, 1968.

Holmgren, L.-A., P. Christopherson, and W. Riedler, On the pitch-angle dependence of auroral electron fluxes in the keV range, *Phys. Norv., 4,* 85, 1970.

Holzer, T. E., The solar wind and related astrophysical phenomena, in *Solar System Plasma Physics,* vol. 1, edited by C. F. Kennel et al., p. 101, North-Holland, New York, 1979.

Iijima, T., and T. A. Potemra, The amplitude distribution of field-aligned currents at northern high latitudes observed by Triad, *J. Geophys. Res., 81,* 2165, 1976.

Kamide, Y., and G. Rostoker, The spatial relationships of field-aligned currents and auroral electrojets to the distribution of night side auroras, *J. Geophys. Res., 82,* 5589, 1977.

Kindel, J. M., and C. F. Kennel, Topside current instabilities, *J. Geophys. Res., 76,* 3044, 1971.

Knight, L., Parallel electric fields, *Planet. Space Sci., 21,* 741, 1973.

Lemaire, J., Impulsive penetration of filamentary plasma elements into the magnetospheres of Earth and Jupiter, *Planet. Space Sci., 25,* 887, 1977.

Lemaire, J., and M. Scherer, Ionosphere-plasma sheet field-aligned currents and parallel electric fields, *Planet. Space Sci., 22,* 1485, 1974.

Longenecker, D., and J. G. Roederer, Polar cap electric field dependence on solar wind and magnetotail parameters, *Geophys. Res. Lett., 9,* 1261, 1981.

Lu, G., P. H. Reiff, J. L. Burch, and J. D. Winningham, On the auroral current-voltage relationship, *J. Geophys. Res., 96,* 3523, 1991.

Lundin, R., Rocket observations of electron spectral and angular characteristics in an "inverted V" event, *Planet. Space Sci., 24,* 499, 1976.

Lundin, R., Processes in the magnetospheric boundary layer, *Phys. Scr., T18,* 85, 1987.

Lundin, R., and I. Sandahl, Some characteristics of the parallel electric field acceleration of electrons over discrete auroral arcs as observed from two rocket flights, Symposium on European Rocket Research, Ajaccio, Corsica, *Eur. Space Agency Spec. Publ., ESA SP-135,* 125, 1978.

Lyons, L. R., Generation of large-scale regions of auroral currents, electric potentials, and precipitation by the divergence of the convection electric field, *J. Geophys. Res., 85,* 17, 1980.

Lyons, L. R., Discrete aurora as the direct result of an inferred, high-altitude generating potential distribution, *J. Geophys. Res., 86,* 1, 1981*a*.

Lyons, L. R., The field-aligned current versus electric potential relation and auroral electrodynamics, in *Physics of Auroral Arc Formation, Geophys. Monogr. Ser.,* vol. 25, edited by S.-I. Akasofu and J. R. Kan, p. 252, AGU, Washington, D. C., 1981*b*.

Lyons, L. R., A simple model for polar cap convection patterns and generation of θ aurora, *J. Geophys. Res., 90,* 2915, 1985.

Lyons, L. R., and O. de la Beaujardiere, Critical problems requiring coordinated measurements of large-scale electric field and auroral distribution, in *Solar Systems Plasma Physics, Geophys. Monogr. Ser.,* vol. 54, edited by J. H. Waite, Jr., et al., p. 399, AGU, Washington, D. C., 1989.

Lyons, L. R., and D. C. Pridmore-Brown, Force balance near an x line in a collisionless plasma, *J. Geophys. Res., 95,* 20,903, 1990.

Lyons, L. R., and R. L. Walterscheid, Generation of auroral omega bans by shear instability of the neutral winds, *J. Geophys. Res., 90,* 12,321, 1985.

Lyons, L. R., and R. L. Walterscheid, Feedback between neutral wind and auroral arc electrodynamics, *J. Geophys. Res., 91,* 13,506, 1986.

Lyons, L. R., and D. J. Williams, *Quantitative Aspects of Magnetospheric Physics,* D. Reidel, Hingham, Mass., 1984.

Lyons, L. R., D. S. Evans, and R. Lundin, An observed relation between magnetic field aligned electric fields and downward electron energy fluxes in the vicinity of auroral forms, *J. Geophys. Res., 84,* 457, 1979.

Lyons, L. R., T. L. Killeen, and R. L. Walterscheid, The neutral wind "flywheel" as a source of quiet-time polar-cap currents, *Geophys. Res. Lett., 12,* 101, 1985.

Lysak, R. L., Electrodynamic coupling of the magnetosphere and ionosphere, *Space Sci. Rev., 52,* 33, 1990.

Maehlum, B. N., and H. Moestue, High temporal and spatial resolution observations of low energy electrons by a mother-daughter rocket in the vicinity of two quiescent auroral arcs, *Planet. Space Sci., 21,* 1957, 1973.

Maezawa, K., Magnetospheric convection induced by the positive and negative Z components of the interplanetary field: Quantitative analysis using polar cap magnetic records, *J. Geophys. Res., 81,* 2289, 1976.

Mansurov, S. M., New evidence of a relationship between magnetic fields in space and on Earth, *Geomagn. Aeron.*, Engl. Transl., *9*, 622, 1969.

Marklund, G. T., et al., A new method to derive "instantaneous" high-latitude potential distributions from satellite measurements including auroral imager data, *Geophys. Res. Lett.*, *14*, 439, 1987.

Maynard, N. C., D. S. Evans, B. Maehlum, and A. Egeland, Auroral vector electric field and particle comparisons, 1, Premidnight convection topology, *J. Geophys. Res.*, *82*, 2227, 1977.

McIlwain, C. E., Direct measurement of particles producing visible aurora, *J. Geophys. Res.*, *65*, 2727, 1960.

Mizera, P. F., and J. F. Fennell, Signatures of electric fields from high and low altitude particle distributions, *Geophys. Res. Lett.*, *4*, 311, 1977.

Mizera, P. F., D. R. Croley, Jr., and J. F. Fennell, Electron pitch-angle distributions in an inverted "V" structure, *Geophys. Res. Lett.*, *3*, 149, 1976.

Nagata, T., and S. Kokubun, An additional daily variation field (S_q') in the polar region on a geomagnetically quiet day, *Rep. Ionos. Space Res. Jpn.*, *16*, 256, 1962.

Nishida, A., N. Iwasaki, and T. Nagata, The origin of fluctuations in the equatorial electrojet; a new type of geomagnetic variation, *Ann. Geophys.*, *22*, 478, 1966.

O'Brien, B. J., Consideration that the source of auroral energetic particles is not a parallel electrostatic field, *Planet. Space Sci.*, *18*, 1821, 1970.

O'Brien, B. J., and D. L. Reasoner, Measurements of highly collimated short-duration bursts of auroral electrons and comparisons with existing models, *J. Geophys. Res.*, *76*, 8258, 1971.

Papadopoulos, K., and T. Coffey, Anomalous resistivity in the auroral plasma, *J. Geophys. Res.*, *79*, 1558, 1974.

Paschmann, G., R. G. Johnson, R. D. Sharp, and E. G. Shelley, Angular distributions of auroral electrons in the energy range 0.8-16 keV, *J. Geophys. Res.*, *77*, 6111, 1972.

Richmond, A. D., and S. Matsushita, Thermospheric response to a magnetic substorm, *J. Geophys. Res.*, *80*, 2839, 1975.

Richmond, A. D., et al., Mapping electrojet features of the high-latitude ionosphere from localized observations: Combined incoherent scatter radar and magnetometer measurements for January 18–19, 1984, *J. Geophys. Res.*, *93*, 5760, 1988.

Rishbeth, H., and O. K. Garriott, *Introduction to Ionospheric Physics*, Academic, San Diego, Calif., 1969.

Roble, R. G., B. A. Emery, R. E. Dickerson, E. C. Ridley, T. L. Killeen, P. B. Hays, B. R. Carigan, and N. W. Spencer, Thermospheric circulation, temperature and compositional structure in the southern hemisphere polar cap during October–November, 1981, *J. Geophys. Res.*, *79*, 9057, 1984.

Roederer, J. G., *Dynamics of Geomagnetically Trapped Radiation*, Springer-Verlag, New York, 1970.

Rossi, R., and S. Olbert, *Introduction to the Physics of Space*, McGraw-Hill, New York, 1970.

Siscoe, G. L., Solar system magnetohydrodynamics, in *Solar-System Physics*, edited by R. L. Carovillano and J. M. Forbes, p. 11, D. Reidel, Hingham, Mass., 1983.

Shelley, E. G., R. D. Sharp, and R. G. Johnson, Satellite observations of an ionospheric acceleration mechanism, *Geophys. Res. Lett.*, *3*, 654, 1976.

Sonnerup, B. U. Ö., Magnetic field reconnection, in *Solar System Plasma Physics III*, edited by L. J. Lanzerotti et al., p. 45, North-Holland, New York, 1979.

Sonnerup, B. U. Ö., On the theory of steady-state reconnection, *Comput. Phys. Commun.*, *49*, 143, 1988.

Speiser, T. W., Conductivity without collisions or noise, *Planet. Space Sci.*, *18*, 613, 1970.

Spitzer, L., Jr., *Physics of Fully Ionized Gases*, 2nd ed., p. 139, Interscience, New York, 1962.

Stern, D. P., A study of the electric field in an open magnetospheric model, *J. Geophys. Res.*, *78*, 7292, 1973.

Svalgaard, L., Sector structure of the interplanetary magnetic field and daily variation of geomagnetic field at high latitudes, *Geophys. Pap. R-6*, Dan. Meteorol. Inst., Copenhagen, Denmark, 1968.

Svalgaard, L., Polar cap magnetic variations and their relationship with the interplanetary sector structure, *J. Geophys. Res.*, *78*, 2064, 1973.

Swift, D. W., and D. A. Gurnett, Direct comparison between satellite electric field measurements and the visual aurora, *J. Geophys. Res.*, *78*, 7306, 1973.

Taylor, H. A., Jr., J. M. Grebowsky, and A. J. Chen, Ion composition irregularities and ionosphere-plasmasphere coupling: Observations of a high latitude ion trough, *J. Atmos. Terr. Phys.*, *37*, 613, 1975.

Temerin, M., M. H. Boehm, and F. S. Mozer, Paired electrostatic shocks, *Geophys. Res. Lett.*, *8*, 799, 1981.

Toffoletto, F. R., and T. W. Hill, Mapping of the solar wind electric field to the Earth's polar caps, *J. Geophys. Res.*, *94*, 329, 1989.

Vallance Jones, A., *Aurora*, D. Reidel, Hingham, Mass., 1974.

Vasyliunas, V. M., Theoretical models of magnetic field line merging, 1, *Rev. Geophys. Space Phys.*, *13*, 303, 1975.

Walterscheid, R. L., and L. R. Lyons, The neutral *E* region zonal winds during intense postmidnight aurora, *J. Geophys. Res.*, *94*, 3703, 1989.

Weimer, R. D., C. K. Goertz, D. A. Gurnett, N. C. Maynard, and J. L. Burch, Auroral electric fields from DE 1 and 2 at magnetic conjunction, *J. Geophys. Res.*, *90*, 7479, 1985.

Weimer, R. D., D. A. Gurnett, C. K. Goertz, J. D. Menietti, J. L. Burch, and Sugiura, The auroral current-voltage relationship in auroral current sheets, *J. Geophys. Res.*, *92*, 187, 1987.

Westerlund, L. H., The auroral electron energy spectrum extended to 45 eV, *J. Geophys. Res.*, *74*, 351, 1969.

Whalen, B. A., and I. B. McDiarmid, Observations of magnetic-field-aligned auroral-electron precipitation, *J. Geophys. Res.*, *77*, 191, 1972.

Whipple, E. C., Jr., The signature of parallel electric fields in collisionless plasma, *J. Geophys. Res.*, *82*, 1525, 1977.

Winningham, J. D., and W. J. Heikkila, Polar cap electron fluxes observed with Isis 1, *J. Geophys. Res.*, *79*, 949, 1974.

Zanetti, L. J., T. A. Potemra, T. Iijima, W. Baumjohann, and P. F. Bythrow, Ionospheric and Birkeland current distributions for northward interplanetary magnetic field: Inferred polar convection, *J. Geophys. Res.*, *89*, 7453, 1984.

L. R. Lyons, Space and Environment Technology Center, M2-260, The Aerospace Corporation, P. O. Box 92957, Los Angeles, CA 90009.